

Enhancing the performance of Praziquantel: an approach using Crystal Engineering and Mechanochemistry

Margarida Gonçalves Susana

Thesis to obtain the Master of Science Degree in

Chemistry

Supervisors: Professor Maria Teresa Nogueira Leal da Silva Duarte

Doctor Vânia Mafalda de Oliveira André

Examination Committee

Chairperson: Professor Isabel Maria Delgado Jana Marrucho Ferreira

Supervisor: Doctor Vânia Mafalda de Oliveira André

Members of the Committee: Professor Maria de Fátima Minas da Piedade

October 2021

Acknowledgements

First, I would like to thank to my supervisors Professor Maria Teresa Duarte and Doctor Vânia André for their guidance and encouragement during this work. Without their support, this thesis would not have been possible.

I want also to express my gratitude to my laboratory colleagues for their helpfulness.

I would like also to thank to Professor Hermínio Diogo, to Doctor Auguste Fernandes for the DSC-TGA and help with FTIR data, as well as to Doctor Luisa Roca Paixão for the computational calculations. Their contribute was of great importance for the complementary of my work.

Additionally, I want to acknowledge the funding from Fundação para a Ciência e a Tecnologia, (projects UIDB/00100/2020, UIDP/00100/2020, and PTDC/QUI-OUT/30988/2017, and FEDER, Portugal 2020 and Lisboa2020 (project LISBOA-01-0145-FEDER-030988), and to COST Action CA18112 for fruitful discussions.

Finally, I want to thank to my family, particularly to my father, and to my friends for their continuous support and constant motivation during this journey. A special thanks to all the friends I met at university for making these 5 years so enjoyable.

Resumo

O Praziquantel (PZQ) é um fármaco anti-helmíntico usado para o tratamento de doenças parasitárias que é considerado essencial pela Organização Mundial de Saúde (OMS). Apesar da sua importância, algumas das suas propriedades físico-químicas não são as mais apropriadas. Aplicando os princípios da engenharia de cristais e da química supramolecular, e usando a mecanoquímica como principal técnica sintética, o objetivo deste projeto é obter cocristais de PZQ com co-formadores orgânicos com o intuito de melhorar as suas propriedades físico-químicas, nomeadamente a solubilidade e estabilidade. Através de moagem assistida por líquido, foram obtidos cocristais de PZQ com ácido salicílico (SAL), 4-aminosalicílico (4-ASA), vanílico (VAN), 4-hidroxibenzóico (4-HBZ), 5-hidroxiisoftálico (5-HIP) e mucónico (MUC) com estequiometria de 1:1; os ácidos 1,2,4,5-benzenotetracarboxílico (BTC) e 3-hidroxibenzóico (3-HBZ) geraram cocristais de PZQ com estequiometria de 2:1, e o ácido trimésico criou cocristais com estequiometria de 1:2. Em todos os cocristais, as interações supramoleculares nas estruturas cristalinas revelaram padrões dominantes de ligações de hidrogénio, especialmente através de ligações O-H...O, N-H...N e N-H...O entre PZQ e os grupos carboxílicos dos co-formadores. Os cocristais obtidos foram caracterizados por difração de raios-X em pó e monocristal, por espectroscopia de infravermelhos com transformada de Fourier e reflectância total atenuada, calorimetria diferencial de varrimento com análise termogravimétrica e por microscopia de placa quente. Foram realizados testes de humidade controlada com teores de humidade relativa de 90 e 83 % para os cocristais que demonstraram estabilidade na bancada. Foram também realizados testes preliminares empíricos de solubilidade, mostrando uma melhoria nesta propriedade quando comparados com o PZQ isolado.

Palavras-chave

Praziquantel, síntese supramoleculares, cocristais, ligações de hidrogénio, mecanoquímica

Abstract

Praziquantel (PZQ) is an anthelmintic drug used for the treatment of parasitic diseases that is considered essential by the World Health Organization (WHO). Despite its importance, some of its physicochemical properties are poor. Applying the principles of crystal engineering and supramolecular chemistry, and using mechanochemistry as the main synthetic technique, the goal of this project is to obtain cocrystals of PZQ with organic coformers, in order to enhance its physicochemical properties, namely solubility and stability. *Via* liquid-assisted grinding (LAG), cocrystals of PZQ with salicylic (SAL), 4-aminosalicylic (4-ASA), vanillic (VAN), 4-hydroxybenzoic (4-HBZ), 5-hydroxyisophthalic (5-HIP) and muconic acid (MUC) were obtained with a 1:1 stoichiometry; 1,2,4,5-benzenetetracarboxylic (BTC) and 3-hydroxybenzoic (3-HBZ) acid formed cocrystals of PZQ with 2:1 stoichiometry, and trimesic acid (TRI) provided cocrystals of PZQ in a 1:2 ratio. In all cocrystals, the supramolecular interactions in the crystal structures revealed dominant hydrogen bonding patterns, specially through O-H \cdots O, N-H \cdots N and N-H \cdots O H-bonds between PZQ and the carboxylic acid moieties of the coformers. The cocrystals obtained were characterized by powder and single-crystal X-ray diffraction (PXRD and SCXRD, respectively), Fourier transform infrared with attenuated total reflectance (FTIR-ATR), combined differential scanning calorimetry (DSC) with thermogravimetric analysis (TGA) and by hot-stage microscopy (HSM). Room humidity tests 90 and 83 % relative humidity contents were performed for cocrystals that showed stability on-shelf. Preliminary empirical solubility tests were also performed, showing an improvement in this property when compared with PZQ alone.

Keywords

Praziquantel, supramolecular synthons, cocrystals, hydrogen bonds, mechanochemistry

Index

Acknowledgements	2
Resumo	3
Abstract.....	4
Index	5
List of Figures	7
List of Tables	10
List of Abbreviations	11
I. Introduction.....	12
1. Developing new pharmaceuticals.....	12
2. Solid forms of pharmaceuticals	12
2.1 Polymorphs, Salts and Cocrystals.....	12
2.2 The Cocrystal World	13
2.2.1 Types of cocrystals.....	14
2.2.2 Properties of cocrystals	14
2.3 Synthesis of cocrystals	15
2.4 Characterization of cocrystals	15
3. Crystal Engineering and Supramolecular Chemistry	16
3.1 Hydrogen bonding	16
3.2 Supramolecular synthon approach.....	16
4. Mechanochemical preparation of cocrystals	17
4.1 Mechanochemical techniques	18
5. Praziquantel.....	19
6. Work outline and goals	20
II. Experimental Section	21
1. Materials	21
2. Synthetic Procedure	21
2.1 Cocrystal Preparation	21
2.2 Single-Crystal Growth.....	23
3. Instrumentation	24

3.1	Powder X-Ray Diffraction (PXRD)	24
3.2	Single-Crystal X-Ray Diffraction (SCXRD)	24
3.3	Fourier Transform Infrared Spectroscopy with Attenuated Total Reflectance (FTIR-ATR) 25	
3.4	Differential Scanning Calorimetry (DSC) and Thermogravimetric Analysis (TGA)	25
3.5	Hot-Stage Microscopy (HSM)	25
4.	Physicochemical Properties Determination	25
4.1	Room Humidity Stability Studies	25
4.2	Preliminary/ Empirical Solubility Studies	26
III.	Results and Discussion	27
1.	Screening of new cocrystals of PZQ	27
2.	Structural characterization of PZQ new crystalline forms	29
2.1	PZQ·SAL	29
2.2	PZQ·4-ASA	32
2.3	PZQ·BTC 2:1	35
2.4	PZQ·VAN	38
2.5	PZQ·3-HBZ 2:1	41
2.6	PZQ·4-HBZ	44
2.7	PZQ·TRI 1:2	47
2.8	PZQ·5-HIP	49
2.9	PZQ·MUC	50
3.	Room Humidity Stability Studies	51
4.	Preliminary/ Empirical Solubility Tests	53
IV.	Conclusions	54
V.	References	55
VI.	Supporting Information	60

List of Figures

Figure 1 Common solid-state approaches for altering API properties and their respective components. Adapted from reference 5.	12
Figure 2 Common types of supramolecular synthons. Adapted from reference 31.	17
Figure 3 Structure of (<i>R,S</i>)-PZQ and its enantiomers. Adapted from reference 45.	19
Figure 4 PXRD patterns for the following samples: PZQ (in blue), SAL (in green), PZQ·SAL prepared by LAG with acetonitrile with 1:1 stoichiometry (in red), and the pattern of PZQ·SAL simulated from the literature (in yellow).	29
Figure 5 Intramolecular and intermolecular hydrogen bonds in PZQ·SAL cocrystal hydrate; (b) supramolecular crystal packing (view along <i>c</i> * axis) of PZQ molecules (in blue), SAL (in green) and water (in red). All non-contact H atoms were omitted for clarity.	30
Figure 6 FTIR-ATR spectra of PZQ (in blue), SAL (in green) and PZQ·SAL (in red).	31
Figure 7 (a) DSC (in red) - TGA (in green) and (b) HSM images for PZQ·SAL.	32
Figure 8 PXRD patterns for the following samples: PZQ (in blue), 4-ASA (in green), PZQ·4-ASA prepared by LAG with acetonitrile with 1:1 stoichiometry (in red), and the pattern of PZQ·4-ASA simulated from the literature (in yellow).	32
Figure 9 (a) Intramolecular and intermolecular hydrogen bonds in PZQ·4-ASA cocrystal solvate; (b) supramolecular crystal packing of PZQ molecules (in green), 4-ASA (in blue) and acetonitrile (in red). All non-contact H atoms were omitted for clarity.	33
Figure 10 FTIR-ATR spectra of PZQ (in blue), 4-ASA (in green) and PZQ·4-ASA (in red).	34
Figure 11 DSC (in red) -TGA (in green) of PZQ·4-ASA.	34
Figure 12 PXRD patterns for the following samples: PZQ (in blue), BTC (in green), PZQ·BTC prepared by LAG with acetonitrile with 1:1 stoichiometry (in purple), PZQ·BTC prepared by LAG with acetonitrile with 2:1 stoichiometry (in red) and the pattern of PZQ·BTC 2:1 simulated from the SCXRD analysis (in yellow).	35
Figure 13 a) Intramolecular and intermolecular hydrogen bonds in PZQ·BTC 2:1 cocrystal; (b) supramolecular crystal packing of PZQ molecules (in green) and BTC (in blue). All non-contact H atoms were omitted for clarity.	36
Figure 14 FTIR-ATR spectra of PZQ (in blue), BTC (in green) and PZQ·BTC 2:1 (in red).	37
Figure 15 (a) DSC (in red) – TGA (in green) and (b) HSM images for PZQ·BTC 2:1.	37
Figure 16 PXRD patterns for the following samples: PZQ (in blue), VAN (in green), PZQ·VAN prepared by LAG with acetonitrile with 1:1 stoichiometry (in red), and the pattern of PZQ·VAN simulated from the literature (in yellow).	38

Figure 17 (a) Intermolecular hydrogen bonds in PZQ·VAN cocrystal; (b) supramolecular crystal packing (view along a axis) of PZQ molecules (in green) and VAN (in blue). All non-contact H atoms were omitted for clarity.	39
Figure 18 FTIR-ATR spectra of PZQ (in blue), VAN (in green) and PZQ·VAN (in red).	40
Figure 19 (a) DSC (in red) – TGA (in green) and (b) HSM images for PZQ·VAN.	40
Figure 20 PXRD patterns for the following samples: PZQ (in blue), 3-HBZ (in green), PZQ·3-HBZ prepared by LAG with acetone with 1:1 stoichiometry (in purple), PZQ·3-HBZ prepared by LAG with acetone with 2:1 stoichiometry (in red) and the pattern of PZQ·3-HBZ 2:1.	41
Figure 21 (a) Intermolecular hydrogen bonds in PZQ·3-HBZ 2:1 cocrystal; (b) supramolecular crystal packing of PZQ molecules (in green and blue) and 3-HBZ (in red). All non-contact H atoms were omitted for clarity.	42
Figure 22 FTIR-ATR spectra for PZQ (in blue), 3-HBZ (in green) and PZQ·3-HBZ 2:1 (in red).	43
Figure 23 (a) DSC (in red) – TGA (in green) and (b) HSM images for PZQ·3-HBZ 2:1.	43
Figure 24 PXRD patterns for the following samples: PZQ (in blue), 4-HBZ (in green), PZQ·4-HBZ prepared by LAG with acetonitrile with 1:1 stoichiometry (in red), and the pattern of PZQ·4-HBZ simulated from the literature (in yellow).	44
Figure 25 (a) Intermolecular hydrogen bonds in PZQ·4-HBZ cocrystal; (b) supramolecular crystal packing (view along a axis) of PZQ molecules (in green) and 4-HBZ (in blue). All non-contact H atoms were omitted for clarity.	45
Figure 26 FTIR-ATR spectra for PZQ (in blue), 4-HBZ (in green) and PZQ·4-HBZ (in red).	46
Figure 27 (a) DSC (in red) – TGA (in red) and (b) HSM images for PZQ·4-HBZ.	46
Figure 28 PXRD patterns for the following samples: PZQ (in blue), TRI (in green), PZQ·TRI prepared by LAG with acetonitrile with 1:1 stoichiometry (in purple), PZQ·TRI prepared by LAG with acetonitrile with 1:2 stoichiometry (in red) and the pattern of PZQ·TRI 1:2 simulated from the SCXRD analysis (in yellow).	47
Figure 29 (a) Intermolecular hydrogen bonds in PZQ·TRI 1:2 cocrystal dihydrate; (b) supramolecular crystal packing of PZQ molecules (in red), TRI (in blue and green) and water (in magenta and yellow). All non-contact H atoms were omitted for clarity.	48
Figure 30 FTIR-ATR spectra for PZQ (in blue), TRI (in green) and PZQ·TRI 1:2 (in red).	49
Figure 31 PXRD patterns for the following samples: PZQ (in blue), 5-HIP (in green) and PZQ·5-HIP prepared by LAG with acetonitrile with 1:1 stoichiometry (in red).	49
Figure 32 FTIR-ATR spectra for PZQ (in blue), 5-HIP (in green) and PZQ·5-HIP (in red).	50
Figure 33 PXRD patterns for the following samples: PZQ (in blue), MUC (in green) and PZQ·MUC prepared by LAG with acetonitrile with 1:1 stoichiometry (in red).	51

Figure 34 Comparison of PXRD patterns for PZQ·4-ASA (in blue) and PZQ·4-ASA after 3 months (in red) on-shelf.	51
Figure 35 Comparison of PXRD patterns for PZQ·MUC (in blue) and PZQ·MUC after 2 months (in red) on shelf.	52
Figure 36 Stability comparison for PZQ·4-ASA (in blue) for 1 (in orange), 2 (in grey), 3 (in yellow) and 7 days (in green) under 90 % RH.	52
Figure 37 Stability comparison for PZQ·4-ASA (in blue) for 1 (in orange), 2 (in grey), 3 (in yellow) and 7 days (in green) under 83 % RH.	53
Figure 38 Solubility comparison for PZQ, PZQ·3-HBZ 2:1, PZQ·4-HBZ, PZQ·TRI 1:2, PZQ·VAN, PZQ·SAL, PZQ·BTC 2:1, PZQ·3-HBZ 1:1 and PZQ·5-HIP (from left to right).....	53

List of Tables

Table 1 Reagents used for the LAG experiments with their CAS-number, chemical supplier, and purity.	21
Table 2 Summary of the coformers and synthetic conditions applied during the cocrystal preparation by LAG.	21
Table 3 Summary of the unsuccessful coformers and synthetic conditions tested.	22
Table 4 Chemical quantity and mass of PZQ and respective conformer used during the synthetic procedure.	22
Table 5 Crystallographic data of PZQ·BTC 2:1, PZQ·3-HBZ 2:1 and PZQ·TRI 1:2.	24
Table 6 Computational calculations' results of the coformers tested that provided cocrystals (in green) and that did not provided cocrystals (in red) when combined with PZQ.	28
Table 7 List of the main hydrogen bonds found for PZQ·SAL cocrystal hydrate.	30
Table 8 List of the main hydrogen bonds found for PZQ·4-ASA cocrystal solvate.	33
Table 9 List of the main hydrogen bonds found for compound PZQ·BTC 2:1.	36
Table 10 List of the main hydrogen bonds found for compound PZQ·VAN.	39
Table 11 List of the main hydrogen bonds found for compound PZQ·3-HBZ 2:1.	42
Table 12 List of the main hydrogen bonds found for compound PZQ·4-HBZ.	45
Table 13 List of the main hydrogen bonds found for compound PZQ·TRI 1:2.	48

List of Abbreviations

4-ASA	4-Aminosalicylic Acid
API	Active Pharmaceutical Ingredient
BCS	Biopharmaceutical Classification System
BTC	1,2,4,5-Benzenetetracarboxylic Acid
CSD	Cambridge Structural Database
DSC	Differential Scanning Calorimetry
FDA	Food and Drug Administration
FTIR-ATR	Fourier Transform Infrared Spectroscopy with Attenuated Total Reflectance
GRAS	Generally Regarded As Safe
3-HBZ	3-Hydroxybenzoic Acid
4-HBZ	4-Hydroxybenzoic Acid
5-HIP	5-Hydroxyisophthalic Acid
HSM	Hot-Stage Microscopy
IR	Infrared
MUC	Muconic Acid
PXRD	Powder X-Ray Diffraction
PZQ	Praziquantel
SAL	Salicylic Acid
SCXRD	Single Crystal X-Ray Diffraction
TGA	Thermogravimetric Analysis
TRI	Trimesic Acid
VAN	Vanillic Acid

I. Introduction

1. Developing new pharmaceuticals

The development of new drugs and their introduction in the market without compromising safety and efficiency is a challenging, time-consuming and an expensive process¹⁻². When developing a novel drug, the focus is to produce a drug with optimal physicochemical properties, high biological activity, and improved therapeutic applications³. However, despite the high number of successfully discovered new drugs, a significant part of them present poor biopharmaceutical properties². In fact, only approximately 40% of approved drugs and almost 90% of the developmental pipeline drugs are molecules with poor solubility based on the definition of the biopharmaceutical classification system (BCS)²⁻⁴. Thus, a promising sustainable development pathway is to find new formulations of already marketed drugs with the aim of improving their pharmaceutical properties.

2. Solid forms of pharmaceuticals

Pharmaceutical cocrystals, salt formation, solvates/ hydrates and polymorphs of active pharmaceutical ingredients (API) are amongst the most common techniques that pharmaceutical companies have been developing to solve properties' related issues^{3,5}. A schematic representation of these possible crystalline forms is presented in Figure 1.

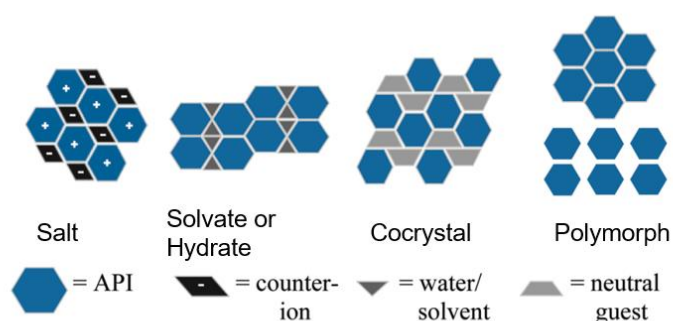


Figure 1 Common solid-state approaches for altering API properties and their respective components. Adapted from reference 5.

2.1 Polymorphs, Salts and Cocrystals

Polymorphism is the ability of a solid material to crystallize in more than one crystalline phase with different arrangements or conformations of the constituents of the crystal lattice, while maintaining the same chemical composition. Since they exhibit different arrangements, their inter- and intramolecular interactions differ, provoking changes in their thermodynamics, kinetic, spectroscopy, surface, packing, mechanical and physicochemical properties, namely solubility and dissolution rate^{3,6}.

Polymorphs can be categorized into conformational and packing. In conformational polymorphism, molecules with different conformations are flexible and exist in the crystalline state. In packing polymorphism, the molecules have the same conformation, however, are packed in a different way in

the three-dimensional space and are quite rigid. Pharmaceutical compounds are generally conformational polymorphs due to the usual flexible moieties in their molecular structures^{6,7}.

In addition, solvates and hydrates are often referred to as pseudo-polymorphs. These solid forms are multicomponent crystalline solid molecular complexes containing the API and a guest molecule incorporated in the crystal lattice structure. When the guest molecule is water, the solid form is denominated hydrate, while solvate refers to molecules with other solvents incorporated⁸.

Salt formation is usually the chosen option regarding enhancing the solubility of pharmaceuticals, therefore, it is estimated that more than half of the drugs are administered as salts. Salts are multicomponent systems where there is proton transference (H^+) from an acid to a base in the ionic state. Apart from the acid and the base, one or more solvents might be involved^{3,6}.

Thus, since there is an H^+ transfer in this process, it is necessary that the API possess a suitable (basic or acidic) ionizable site⁵. In addition, the extent of H^+ transfer is defined by the “ ΔpK_a rule” (pK_a of base - pK_a of acid) in solution and the crystalline environment⁶.

When compared to salts, cocrystals involve no H^+ transfer, as both the API and the cocrystal former are neutral substances. Therefore, any API could potentially form cocrystals regardless having acidic, basic or ionizable groups^{3,5}.

Since the work developed within this thesis is centered in obtaining cocrystals, these solid forms will be discussed in detail in the next section 2.2 from chapter I. Introduction.

2.2 The Cocrystal World

In the last two decades, the research on cocrystals has gained massive attention among scientists due to being one of the major targets in the search for new materials with novel or improved supramolecular properties⁹⁻¹⁰. In fact, the beginning of this new area in crystal engineering and cocrystal formation started when, in 2004, pharmaceutical cocrystals were described as a different class of novel and crystalline materials capable of changing the physicochemical properties of APIs¹¹⁻¹². With that being said, pharmaceutical cocrystals are designed to optimize a property of interest. For example, if the API is too soluble or too insoluble, a proper cocrystal can be designed to decrease or increase its solubility¹³.

According to literature, the definition of cocrystal has not always been consensual. In 2012, during the Indo-US Bilateral Meeting sponsored by the Indo-US Science and Technology Forum, 46 scientists proposed a broad definition of cocrystal that was consistent with the scientific literature: *“Cocrystals are solids that are crystalline single phase materials composed of two or more different molecular and/or ionic compounds generally in a stoichiometric ratio which are neither solvates nor simple salts”*^{11,14}. Thus, FDA defines pharmaceutical cocrystals as “crystalline materials composed of two or more different molecules, typically API and cocrystal formers (coformers), in the same crystal lattice”^{9,14}. This coformer must be inherently safe for use in a drug product, *i.e.* those with the Generally Regarded As Safe (GRAS) designation¹⁵, and both the API and the coformer(s) must be solid under ambient conditions⁹. The assembly between cocrystal’s components is done *via* non-covalent interactions, namely hydrogen bonds (H-bonds), π - π or van der Waals interactions³.

2.2.1 Types of cocrystals

Cocrystals can be classified according to the nature of the coformers as “molecular” or “ionic” cocrystals¹⁴. Molecular cocrystals (MCCs) contain two or more different neutral (or non-ionized) coformers in a stoichiometric ratio that are typically sustained by hydrogen or halogen bonds, representing the majority of the cocrystals reported. Ionic cocrystals (ICCs) are in a stoichiometric ratio and, typically, are sustained by charge assisted hydrogen bonds and/or coordination bonds (if metal cations are present)^{11,14}. These ICCs usually are formed by an organic molecule and an inorganic alkaline or alkaline earth salt, combining the characteristics of molecular crystals with those typical of ionic salts, i.e., thermal stability and solubility in water¹⁶.

2.2.2 Properties of cocrystals

As mentioned already, cocrystals can optimize the physicochemical properties of the APIs. One advantage of these compounds is that they are stable crystalline forms, and, in their formulations, there is no need of other excipients and additives^{11,17}. When formulating cocrystals, the APIs will have their physicochemical properties improved due to the presence of coformers in the crystal structure, being that these properties depend on the available coformer^{5,11}.

2.2.2.1 Melting Point

Melting point is defined by the temperature at which the solid and the liquid phase are in equilibrium, being used to determine the purity of compounds with sharp melts and narrow ranges^{5,11}. The value is calculated from the ratio of the total phase change in the enthalpy and entropy of fusion¹⁸ and the preferred technique to characterize this property should be the differential scanning calorimetry (DSC) and thermal gravimetric analysis (TGA).

Higher melting point refer to higher thermodynamical stability, and, for this reason, it is possible to increase the thermal stability of an API by choosing a coformer with higher melting point to form the cocrystal. However, when dealing with thermolabile drugs, it could be advantageous to select coformers with lower melting point¹¹.

2.2.2.2 Solubility

Trying to improve this property is one of the main reasons why the research on cocrystals has gained such a huge attention. However, enhancing aqueous solubility without compromising stability is undoubtedly a big challenge.

Cocrystal's solubility is affected by the solubility of the API and the coformer, as well as polarity of the solvent system, temperature, and pH¹⁹. Since there are many hydrophobic drugs in the market, which results in poor absorption, low bioavailability, and solubility, most of the pharmaceutical cocrystals are composed of a hydrophobic drug and a hydrophilic coformer²⁰.

To dissolve cocrystals, it is necessary to break their intermolecular bonds, as well as break the intermolecular bonds in the solvent and then form new bonds between cocrystal and solvent molecules. Therefore, solubility of cocrystals depends on the strength of intermolecular interactions in the crystal lattice and solvation of cocrystal components. By combining the APIs with coformers, coformers seem

to decrease the solvation barrier of cocrystals, increasing the solubility¹⁹⁻²⁰. One example of this theory was proved by Mihaela M. Pop *et al.* that reported a that “100-fold solubility increase in water was obtained by ketoconazole co-crystallization with fumaric and adipic acid”²¹.

2.2.2.3 Stability

Apart from solubility, the stability of the drug is its most important physicochemical property. The drug can be considered as stable when it is able to preserve its physical, chemical, biological, therapeutic and microbial properties when stored and used. However, it can be influenced by many factors such as temperature, pH, variations in the solubility and the moisture content. Moisture is an important parameter to monitor because water catalyzes some chemical reactions, such as redox reactions and hydrolysis. For this reason, studies in relative humidity stress are usually performed to determine the effect of water on the formulation^{3,11}.

The powder X-ray diffraction (PXRD) data is collected at the end of the moisture balance experiment providing information about the final form and compared to the initial data; In order to track possible phase conversions, data should be collected in shorter time intervals instead of only once at the beginning and the end of a longer time interval⁵.

2.3 Synthesis of cocrystals

The traditional techniques used to synthesize cocrystals are solution-based and solid-state methodologies.

Regarding solution-based methods, there are many different options, such as solvent evaporation, solution crystallization, antisolvent addition, slurry conversion and the reaction crystallization method²². Of note is the solvent evaporation method, which is the most used. In this technique, the API and the coformer are dissolved in solvent, leaving it to evaporate slowly¹¹. Also, the slurry conversion method is often used, presenting the benefit of not requiring a fully dissolved starting solution, contrary to most solution-based methods, and implies the suspension of both reagents, in excess, in a solvent²³.

Among solid-state methods, mechanochemical synthesis of cocrystals has gained significant interest lately because, with this technique, it is possible to synthesize cocrystals in the absence of solvent, or by using negligible amounts of solvent, and yet obtain excellent purity and quality results²⁴. And of utmost importance, it is possible to obtain new products while using highly insoluble APIs, and most of them are in this class of compounds. Since mechanochemistry was the synthetic approach used in this work, this subject will be discussed in further detail in section 4 of chapter I. Introduction.

2.4 Characterization of cocrystals

Among other analytical techniques, the structural characterization of cocrystals can be performed recurring to powder and single-crystal X-ray diffraction (PXRD and SCXRD, respectively), Fourier-transform infrared (FTIR) spectroscopy, differential scanning calorimetry (DSC), thermogravimetric analysis (TGA) and hot-stage microscopy (HSM).

However, to design, synthesize and characterize new cocrystals, it is necessary to understand their intermolecular interactions, which will be discussed in the next section.

3. Crystal Engineering and Supramolecular Chemistry

In the crystal engineering context, the first step is to understand the interactions that sustain and direct crystal packing. The intermolecular interactions in these crystalline structures involve the hydrogen bond, including its weakest variant, the C-H... π interaction, van der Waals interactions, dipole-dipole interactions, and the halogen bond^{13,25}. In cocrystals, both cocrystal formers interact with each other by non-covalent bonding mostly by hydrogen bonding¹¹.

3.1 Hydrogen bonding

Hydrogen bonds are the primary design elements in multicomponent pharmaceutical cocrystals. In 1991, Etter²⁶ acknowledged three general rules applied to organic hydrogen-bonded structures:

- All good proton donors and acceptors are used in hydrogen bonding;
- If six-membered ring intramolecular hydrogen bonds can form, they will usually do so in preference to forming intermolecular hydrogen bonds;
- The best proton donors and acceptors remaining after intramolecular hydrogen-bond formation form intermolecular hydrogen bond to one another, establishing covalent bonds.

3.2 Supramolecular synthon approach

When choosing the coformer suitable for supramolecular interaction with the API, the first can be selected based on complementarity of molecular recognition sites^{13,27}. In 1995, Desiraju²⁸ described the "synthon approach" for the selection of coformers which formed a supermolecule by using certain molecular fragments within the cocrystal to create "supramolecular synthons". These supramolecular synthons *"are structural units within supermolecules which can be formed and/or assembled by known or conceivable synthetic operations involving intermolecular interactions"*²⁸. When designing these supramolecular structures, the goal is to develop synthons that are robust enough to be exchanged from one network structure to another, being present in the supermolecules as basic structural units which are associated with non-covalent bonding^{11,28}. Robust synthons are formed with strong and directional interactions and once formed, they do not have the tendency to break¹³.

3.2.1 Types of synthons

Synthons that are based upon hydrogen bonds represent a prototypal tool for crystal engineering and can be classified in two types: supramolecular homosynthons and supramolecular heterosynthons. Homosynthons are designed by same functional groups present in the API and the coformer, self-complementary moieties, i.e., dimers formed by carboxylic acids and amide homodimers. In contrast, heterosynthons are formed by different functions groups but complementary functional groups, i.e., carboxylic acid-amide and carboxylic acid-pyridine heterosynthons^{11, 29-30}. These last ones are generally more favored than homosynthons, i.e., the acid-amide and the acid-pyridine heterosynthons are commonly used in comparison with the carboxylic acid and amide homodimers. Despite the complementary hydrogen bond donor and acceptor sites in homosynthons, its formation is unlikely in competitive situations^{11,31}. In Figure 2 are represented the most common types of synthons in cocrystals.

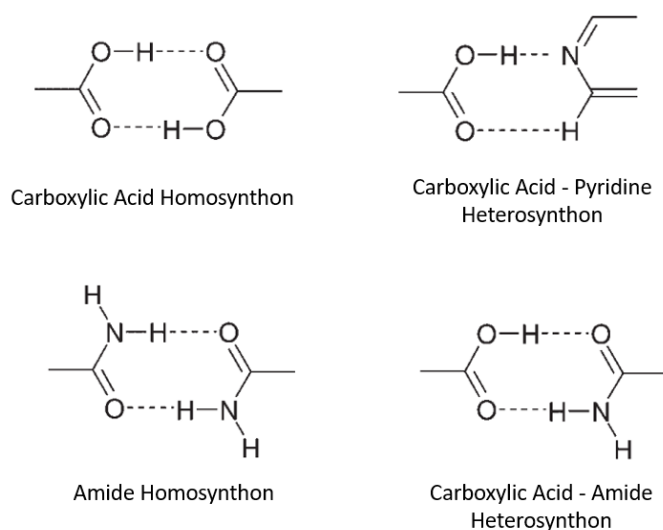


Figure 2 Common types of supramolecular synthons. Adapted from reference 31.

3.2.2 Graph-set analysis of hydrogen-bonding

In order to describe hydrogen bond patterns, Etter and coworkers³² proposed a graph-set notation to simplify these interactions:

$$G_d^a(r)$$

Graph-sets are descriptors that tell how many donors and acceptors used in a H-bond and the nature of the pattern. In this model, G is the descriptor referring to the pattern of H-bonding, r is the number of H atoms involved, a the number of acceptors and d is the number of donors.

Regarding the descriptors, S (which stands for self) denotes intramolecular H-bonds. For intermolecular H-bonds, the descriptor can be represented by C , which refers to H-bonded chains that are infinite; D , that refers to noncyclic dimers; and R , which refers to rings³². Of note is the synthon $R_2^2(8)$, represented in Figure 2 by the carboxylic acid homosynthon, which is one of the most common type of synthons in crystal engineering.

Using the Cambridge Structure Database (CSD)³³ it is possible to perform research of already existing crystal structures and, therefore, an analysis of their packing motifs and how they form supramolecular synthons, being this step fundamental to initiate a crystal engineering experiment³¹. CSD is a computerized database of small organic and metal-organic structures determined by diffraction methods. It includes bibliographic, chemical, and physical information, as well as accurate 3D structures of the crystal data deposited³³.

4. Mechanochemical preparation of cocrystals

Considering the crystal engineering field, mechanochemistry is nowadays a common approach to the synthesis of cocrystals and metal organic frameworks (MOFs), being identified by IUPAC as one of the 10 world-changing technologies³⁴⁻³⁷. Mechanochemistry is a term applicable for reactions that use

mechanical energy to facilitate chemical transformations, and it is seen as an great method of Green Chemistry since the reactions are carried out without any solvent or in the presence of catalytic amounts of solvent^{34,36}. In recent years this technique has gained increasing interest for the synthesis of novel compounds, emerging from the need of pharmaceutical and chemical industries for cleaner, safer, and more efficient transformations, which also provides beneficial economic and ecological features. In general, mechanochemistry can provide some advantages in relation to solution-based techniques such as shorter reaction times, higher product yields, the removal of unsafe and excessive organic solvents, unique reactivity, and selectivity, and opens the possibility towards numerous compounds that cannot be obtained by other synthetic techniques^{35,38-39}.

Mechanochemistry uses mechanical energy imposed by grinding, shearing, stretching, or milling for inducing chemical transformations and these methods can be performed manually or by a non-manual way³⁹⁻⁴⁰. Historically, manual grinding using a mortar and pestle was the first technique applied for mechanical activations of chemical systems. However, this method can cause safety issues, low reproducibility and can have some scale-up limitations. In addition, this method may be extremely slow, making it only feasible for transformations that require short reaction times^{39,41}. For that reason, the use of ball-milling techniques has gained emphasis as it enables the control of parameters such as the frequency and energy input (milling time), ensuring higher reproducibility³⁹. With this procedure, in which moving balls applies kinetic energy to the material, chemical bonds are broken by fracturing material particles, allowing the formation of new bonds⁴².

4.1 Mechanochemical techniques

Regarding mechanochemistry, several techniques can be applied according to the amount (or absence) of solvent used in the process, among which neat and liquid-assisted grinding stand out.

4.1.1 Neat grinding

The simplest mechanochemical way for cocrystalization is by neat grinding of two or more cocrystal components⁴⁰. This technique involves the combination of the reagents in their dry solid form with the application of pressure, through manual or mechanical means. No solvent is added in this procedure²³.

4.1.2 Liquid-assisted grinding (LAG)

The parameter η can be used to characterize LAG reactions and as a way of comparison with other synthetic techniques, i.e. in neat grinding, $\eta=0$, and in solution reactions, $\eta=12\text{ }\mu\text{L mg}^{-1}$ or more. In this technique, a small amount ($\eta=0\text{-}2\text{ }\mu\text{L mg}^{-1}$) of liquid is introduced into a milling jar along with the reactants and the balls, allowing to control the chemical selectivity. LAG is usually the preferred mechanochemistry method as the solvent can accelerate or even enable reactions that do not occur by neat grinding^{36,39}.

4.1.3 Ion- and Liquid-assisted grinding (ILAG) and Polymer-assisted Grinding (POLAG)

ILAG was developed from LAG to allow the direct conversion of mineral-like feedstocks into metal-organic materials. In this technique, small amounts of salt (5 mol % or less) and a liquid are used to activate systems that react only partially or not at all by LAG. While neat grinding can have limited extent

when synthesizing MOFs, ILAG can give rapid and quantitative formation of a series of close-packed or open-frameworks since the grinding liquid and the ionic salt act as catalyst^{36,40}.

Using liquid or solid polymers instead of organic solvents can be useful to avoid solvate formation in LAG cocrystalization. Polymers such as polyethylene glycols (PEGs) can also be used as catalysts to accelerate cocrystalization and direct the formation of polymorphs as well as to control product particle size³⁶.

5. Praziquantel

The API used in this work was Praziquantel (PZQ). PZQ, (*RS*)-2-(cyclohexylcarbonyl)-1,2,3,6,7,11b-hexahydro-4*H*-pyrazino[2,1-*a*]isoquinolin-4-one (Figure 3). It was developed by E. Merck and Bayer AG, in 1975, and it is used in human and veterinary medicine as an anthelmintic drug for the treatment of parasitic diseases caused by cestodes and trematodes. This drug is the only one commercially available to treat schistosomiasis in humans, an infection caused by flatworms, and, for that reason, it is included in the World Health Organization (WHO) Model List of Essential Drugs⁴³⁻⁴⁴.

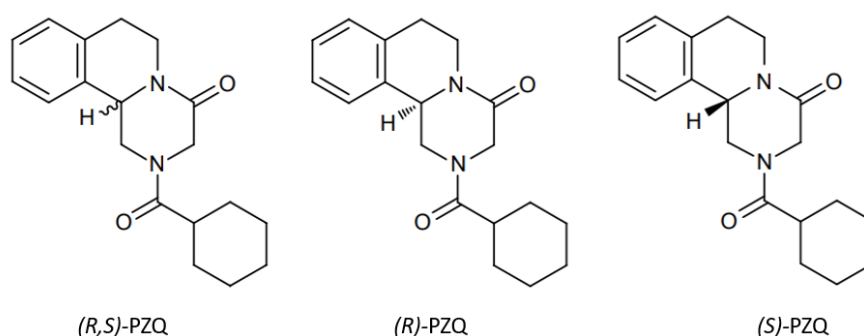


Figure 3 Structure of (*R,S*)-PZQ and its enantiomers. Adapted from reference 45.

PZQ is synthesized and administered in the racemic form, (*RS*)-PZQ. However, only the (*R*)-enantiomer is active and has the desired therapeutic activity, while the (*S*)-enantiomer is associated with some undesirable side effects⁴⁶. In addition, this drug must be administered in high doses, with a human dose containing 600 mg of the API, due to its poor aqueous solubility (0.40 mg/ mL at 25 °C). Thus, PZQ is classified as a BCS class II drug because of its low solubility and high permeability^{19,43,46-47}. Therefore, the use of PZQ is limited, and hence the need to discover and identify new solid forms, such as polymorphs, hydrates or cocrystals in order to improve its weak physicochemical and biopharmaceutical properties is strengthened^{43,48}.

Despite the need to enhance PZQ's properties, there are not many cocrystals of this API reported yet, as it can be proven through research on CSD³³. In fact, in 2013, Herbert Höpfl and coworkers⁴³ reported nine cocrystals of PZQ with fumaric, pimelic, adipic, maleic, oxalic, succinic, malonic and glutaric acids. These structures can be retrieved from CSD with the refcodes TELBUJ, TELCAQ, TELCIY, TELCOE, TELDAR, TELDEV, TELDIZ, respectively. In February 2021, Li Zhang *et al.*⁴⁹ published their work where

they report cocrystals of PZQ with three flavonols, whose refcodes are ANAYOG, ANAYUM and ANAZAT. Finally, and already during the work of this thesis, René de Gelder⁴⁸ reported twelve cocrystals of PZQ with benzoic acid derivatives and aromatic compounds with hydroxyl, amine, and nitro-groups, whose CSD refcodes are AVEHER, AVEHIV, AVEHOB, AVEHUH, AVEJAP, AVEJET, AVEJIX, AVEJOD, AVEJUJ, AVEKAQ, AVEKEU and AVEKIY.

6. Work outline and goals

Using the principles of crystal engineering and supramolecular chemistry, the goal of this project was to obtain cocrystals of PZQ, and therefore to enhance its physicochemical properties (namely solubility and stability). The main synthetic technique used during the work was mechanochemistry, and the cocrystals obtained were characterized by PXRD and SCXRD, FTIR-ATR, combined DSC-TGA and HSM.

II. Experimental Section

1. Materials

All reagents and solvents used in this work were purchased from Sigma-Aldrich, Fluka, Alfa Aesar and TCI Chemicals and used as received without further purification. In Table 1 are summarized the reagents used with their respective CAS-numbers, chemical supplier, and purity degree.

Table 1 Reagents used for the LAG experiments with their CAS-number, chemical supplier, and purity.

Reagent	CAS-number	Supplier	Purity
Praziquantel	55268-74-1	Sigma-Aldrich	>98%
		TCI Chemicals	>98%
Trimesic Acid	554-95-0	Fluka	>97%
trans,trans-Muconic Acid	3588-17-8	Sigma-Aldrich	98%
Salicylic Acid	69-72-7	Fluka	>99%
4-Aminosalicylic Acid	65-49-6	Sigma-Aldrich	99%
5-Hydroxyisophthalic Acid	618-83-7	Sigma-Aldrich	97%
1,2,4,5-Benzenetetracarboxylic Acid	89-05-4	Sigma-Aldrich	96%
Vanillic Acid	121-34-6	Alfa Aesar	98%
3-Hydroxybenzoic Acid	99-06-9	Sigma-Aldrich	99%
4-Hydroxybenzoic Acid	99-96-7	Sigma-Aldrich	99%

2. Synthetic Procedure

2.1 Cocrystal Preparation

LAG experiments were performed in a Retsch MM400 mixer mill operated at a frequency of 25 Hz using stainless steel grinding jars (10 mL). Before starting, 40 μ L of solvent (acetonitrile, acetone, or ethanol) and two balls of 7 mm each were added to approximately 200 mg of mixture with the correspondent stoichiometric ratio. Table 2 summarizes the conditions of the synthetic procedure.

Table 2 Summary of the cofomers and synthetic conditions applied during the cocrystal preparation by LAG.

Cocrystal former	Stoichiometry PZQ/Cocrystal former	Solvent	Reaction time (min)
Trimesic Acid (TRI)	1:2	CH ₃ CN	30
trans,trans-Muconic Acid (MUC)	1:1	CH ₃ CN	30
Salicylic Acid (SAL) *1	1:1	CH ₃ CN	30
		C ₂ H ₆ O	45
4-Aminosalicylic Acid (4-ASA)	1:1	CH ₃ CN	30
5-Hydroxyisophthalic Acid (5-HIP)	1:1	CH ₃ CN	30
1,2,4,5- Benzenetetracarboxylic Acid (BTC)	2:1	CH ₃ CN	30
Vanillic Acid (VAN)	1:1	CH ₃ CN	45
3-Hydroxybenzoic acid (3-HBZ)	2:1	C ₃ H ₆ O	30

4-Hydroxybenzoic Acid (4-HBZ)	1:1	CH ₃ CN	30
L- (+)-Tartaric Acid (TAR) *2	1:1	CH ₃ CN	30
Oxalic Acid (OXA) *3	1:1	C ₃ H ₆ O	30

*1 same cocrystal obtained for the two different solvents

*2 not reproducible

*3 conditions of the reaction were not optimized

In addition to these coformers that provided new crystalline forms when combined with the API used in this work, other coformers were tested, however no new forms were obtained by the applied synthetic conditions presented in Table 3. All the following experiments were also performed using stainless steel grinding jars of 10 mL with two balls of 7 mm each for total mixtures of 200 mg.

Table 3 Summary of the unsuccessful coformers and synthetic conditions tested.

Cocrystal former	Stoichiometry PZQ/Cocrystal former	Solvent	Reaction time (min) and frequency (Hz)
Terephthalic Acid	1:1	C ₃ H ₆ O (40 and 60 μ L)	30 at 25 Hz
		CH ₃ CN (40 μ L)	30 at 25 Hz
Oxalic Acid	1:1	C ₃ H ₆ O (60 μ L)	30 at 25 Hz
		CH ₃ CN (40 μ L)	30 at 25 Hz
Isophthalic Acid	1:1	CH ₃ CN (40 μ L)	15 at 29.5 Hz
Citric Acid	1:1	CH ₃ CN (40 μ L)	30 at 25 Hz
		H ₂ O (40 μ L)	30 at 25 Hz
L-Glutamic Acid	1:1	CH ₃ CN (40 μ L)	30 at 25 Hz
Aspirin	1:1	CH ₃ CN (40 μ L)	30 at 25 Hz
Nicotinic Acid	1:1	CH ₃ CN (40 μ L)	30 at 25 Hz
4-Aminobenzoic Acid	1:1	CH ₃ CN (40 μ L)	30 at 25 Hz
3-Aminobenzoic Acid	1:1	CH ₃ CN (40 μ L)	30 at 25 Hz
Benzoic Acid	1:1	CH ₃ CN (40 μ L)	30 at 25 Hz
Biphenyl-4,4-dicarboxylic Acid	1:1	CH ₃ CN (40 μ L)	30 at 25 Hz
Tricarballic Acid	1:1	CH ₃ CN (40 μ L)	30 at 25 Hz
4-Aminosalicylic Acid	1:1	C ₃ H ₆ O (40 μ L)	30 at 25 Hz
		C ₂ H ₆ O (40 μ L)	30 at 25 Hz
3-Hydroxybenzoic Acid	1:1	CH ₃ CN (40 μ L)	30 at 25 Hz

In a more advanced phase of the work, experiments using total mixtures of 400 mg were performed to figure if the reaction would still occur (scale-up process). These experiments were done in 25 mL grinding jars with 80 μ L of solvent being added to the reagents, while the stoichiometric ratio of PZQ-coformer and the number/size of the balls remained the same.

Below, in Table 4, are summarized the chemical quantity (n) and the mass (m) of the API and coformer weighted for the mechanochemical procedure with total mixtures of 200 mg.

Table 4 Chemical quantity and mass of PZQ and respective conformer used during the synthetic procedure.

Cocrystal	n PZQ (mmol)	m PZQ (mg)	n Coformer (mmol)	m Coformer (mg)
-----------	-----------------	---------------	----------------------	--------------------

PZQ·TRI 1:2	0.276	86.1	0.552	116.0
PZQ·MUC	0.443	138.3	0.443	63.0
PZQ·SAL	0.449	140.3	0.447	61.7
PZQ·4-ASA	0.433	135.2	0.432	66.2
PZQ·5-HIP	0.407	127.1	0.407	74.1
PZQ·BTC 2:1	0.467	145.9	0.229	58.1
PZQ·3-HBZ 2:1	0.526	164.4	0.265	36.6
PZQ·VAN	0.420	131.2	0.420	70.6

2.2 Single-Crystal Growth

Crystals of the new cocrystals suitable for single crystal X-ray diffraction analysis were obtained by two different methods: (i) Cocrystals of PZQ·SAL, PZQ·4-ASA, PZQ·BTC, PZQ·VAN, PZQ·3-HBZ and PZQ·4-HBZ were obtained by recrystallization of the kneading product in a solvent saturated solution by slow evaporation of the solvent at room temperature; (ii) PZQ·TRI 1:2 cocrystals were obtained by mixing the reagents in a solvent solution, with the reaction yielding directly single crystals.

2.2.1 PZQ·SAL – Cocrystal hydrate of PZQ, SAL and water

A small amount of the white powder obtained by the mechanochemical reaction was dissolved in a solution containing distilled water and ethanol (approx. 10 mL total, 50:50 v:v) heated up to 40°C during approx. 30 min. The slow evaporation of the solution, at room temperature, resulted in colorless plate-like crystals after 14 days.

2.2.2 PZQ·4-ASA – Cocrystal solvate of PZQ, 4-ASA and acetonitrile

A small amount of the white powder obtained by the mechanochemical reaction was dissolved in acetonitrile at 40°C, for approx. 30 min. After 14 days, colorless block-shape crystals were obtained.

2.2.3 PZQ·BTC 2:1 – Cocrystal of PZQ and BTC

A small amount of the white powder obtained after grinding was dissolved in acetonitrile at 40°C. Since the product was not dissolving completely after approx. 15min, a few drops of water were added to the solution and stirred for more 15 min approx. before taken out. After 5 days, colorless block-like crystals were obtained by slow evaporation.

2.2.4 PZQ·VAN – Cocrystal of PZQ and VAN

A small amount of the white powder obtained was dissolved in a solution containing distilled water and ethanol (approx. 10 mL total, 50:50 v:v) heated up to 40°C during approx. 30 min. After 15 days, colorless needle-like crystals were obtained.

2.2.5 PZQ·3-HBZ 2:1 – Cocrystal of PZQ and 3-HBZ

A small amount of the white powder obtained was dissolved in a minimum amount of acetone. Since the solvent evaporated very quickly, the next day more acetone was added. After 12 days, 2 mL of diethyl ether and a few drops of water were added to the resulting solution and mixed for approx. 20 min. After 2 days, colorless plate-like crystals were obtained.

2.2.6 PZQ·4-HBZ – Cocrystal of PZQ and 4-HBZ

For this new form, the same cocrystal suitable for single-crystal X-ray diffraction was obtained by two different ways. In the first one, a small amount of the powder obtained was dissolved in hot acetonitrile (40°C) for approx. 5 min, while in the second way, the powder was dissolved in a minimum amount of acetone. In both cases colorless block-like crystals were obtained after 6 days by slow evaporation of the solvent.

2.2.7 PZQ·TRI 1:2 – Cocrystal dihydrate of PZQ, TRI and water

An equimolar mixture of PZQ (30.3 mg) and trimesic acid (20.8 mg) was dissolved in a solution with 3.5 mL of ethyl acetate and 3.5 mL of n-heptane. The solution was heated up to 40°C for approx. 20 min and, after 7 days, colorless plate-like crystals were obtained on top of the solvent.

3. Instrumentation

3.1 Powder X-Ray Diffraction (PXRD)

Room temperature powder X-ray diffraction (PXRD) data were collected on a D8 Advance Bruker AXS θ -2 θ , diffractometer equipped with a LYNXEYE-XE detector, copper radiation source (Cu K α , λ = 1.5406 Å), operated at 40 kV and 40 mA. It was used to ascertain the bulk material purity of compounds synthesized by comparing the calculated (in MERCURY 2021.2.0⁵⁰ from SCXRD data) and experimental PXRD patterns. Data was collected in the 3-60° range in 2 θ , with a step size of 0.02°. Throughout the measurements, nickel filter was used in the data collection.

3.2 Single-Crystal X-Ray Diffraction (SCXRD)

Crystals suitable for single X-ray diffraction studies were mounted on a loop with Fomblin® protective oil. Data were collected on A Bruker AXS-KAPPA D8 - QUEST, with graphite-monochromated radiation (Mo K α , λ = 0.71073 Å), at 293 K. X-ray generator was operated at 50 kV and 30 mA and APEX3 program monitored the data collections. Data were corrected for Lorentzian polarization and absorption effects using SAINT⁵¹ and SADABS⁵² programs. SHELXT 2014/4⁵³ was used for structure solution and SHELXL 2014/7⁵³ was used for full matrix least-squares refinement on F². These two programs are included in the WINGX-Version 2014.1⁵⁴ program package. A full-matrix least-squares refinement was used for the non-hydrogen atoms with anisotropic thermal parameters. Hydrogens were inserted in idealized positions and allowed to refine in the parent carbon atom, except the water hydrogen atoms that were located from the electron density map and the distances were restrained. MERCURY 2021.2.0⁵⁰ was used for packing diagrams. PLATON⁵⁵ was used for determination of hydrogen bond interactions. Table 5 summarizes data collection and refinement details.

Table 5 Crystallographic data of PZQ·BTC 2:1, PZQ·3-HBZ 2:1 and PZQ·TRI 1:2.

Structure	PZQ·BTC 2:1	PZQ·3-HBZ 2:1	PZQ·TRI 1:2
Chemical Formula	C ₄₂ H ₅₄ N ₄ O ₁₂	C ₄₅ H ₅₄ N ₄ O ₇	C ₃₇ H ₃₅ N ₂ O ₁₆
Molecular Weight	878.95 g/mol	762.92 g/mol	737.67 g/mol
Crystal form,	Block-shape, colorless	Plate-like, colorless	Plate-like, colorless

Color			
Crystal Size (mm)	0.180 x 0.100 x 0.080	-	-
Crystal System	Triclinic	Triclinic	Monoclinic
Space group	<i>P</i> -1	<i>P</i> 1	<i>C</i> 2/ <i>c</i>
<i>a</i> (Å)	9.5037(11)	6.2139(6)	16.49(4)
<i>b</i> (Å)	10.5666(13)	9.6836(9)	34.59(8)
<i>c</i> (Å)	12.6738(13)	17.2147(17)	14.00(4)
α (°)	108.196(4)	90.689(4)	90
β (°)	103.340(4)	95.127(4)	116.82(6)
γ (°)	106.032(3)	105.817(4)	90
<i>V</i> (Å³)	1089.8(2)	991.93(17)	7128(30)
<i>Z</i>	1	1	8
<i>d</i> (mg/m³)	1.339	1.277	1.423
μ (mm⁻¹)	0.097	0.086	0.113
θ range (°)	1.804-26.500	2.187-33.293	2.011-25.838
Reflections collected/unique	48372/ 4467	73675/ 15154	562937 6806
<i>R</i>_{int}	0.1112	0.2206	0.1630
Goodness-of-fit on <i>F</i>²	1.024	0.967	1.231
Final <i>R</i> indices^{a,b} [<i>I</i> > σ(<i>I</i>)]	<i>R</i> ₁ =0.1023, <i>wR</i> ₂ =0.2465	<i>R</i> ₁ =0.0749, <i>wR</i> ₂ =0.1722	<i>R</i> ₁ =0.1252, <i>wR</i> ₂ =0.3535

3.3 Fourier Transform Infrared Spectroscopy with Attenuated Total Reflectance (FTIR-ATR)

The FTIR spectra were obtained in reflectance mode using a Thermo Nicolet 6700 spectrometer with attenuated total reflectance (ATR). The measurements were recorded in the range of 650-4000 cm⁻¹, 64 scans, and applying background and atmosphere correction when needed.

3.4 Differential Scanning Calorimetry (DSC) and Thermogravimetric Analysis (TGA)

Combined TGA-DSC measurements were carried out on a SETARAM TG-DTA 92 thermobalance under nitrogen flow with a heating rate of 10 °C /min. The samples weights were in the range 10-20 mg.

3.5 Hot-Stage Microscopy (HSM)

Hot-stage experiments were carried out using a Linkam TP94 device connected to a Linkam LTS350 platinum plate. Images were collected, via the imaging software Cell, with an Olympus B061 microscope. The crystals were placed on an oil drop to allow a better visualization of solvent or decomposition products release.

4. Physicochemical Properties Determination

4.1 Room Humidity Stability Studies

The new forms obtained by mechanochemistry (except PZQ·MUC) were placed in two different sealed with high vacuum grease desiccators: one containing a saturated solution of potassium nitrate (KNO₃) and the other containing a saturated solution of sodium chloride (NaCl). These solutions were able to

maintain the environment of the desiccators with a relative humidity (RH) content of 90% and 83%, respectively. PZQ·SAL, PZQ·BTC 2:1, PZQ·VAN, PZQ·3-HBZ 2:1 and PZQ·4-HBZ powders were left inside the desiccators and their PXRD diffractograms were taken after 1, 14, 21 and 70 days; PZQ·4-ASA was also analyzed after 7 days, while PZQ·5-HIP and PZQ·TRI 1:2 were analyzed only twice: after 24 and 48 h. PXRD diffractograms were analyzed to detect possible changes in the powder diffraction patterns. Whenever changes were noticed, it was assumed that structural transformations had occurred, and therefore, the stability of the cocrystal was compromised.

4.2 Preliminary/ Empirical Solubility Studies

Preliminary solubility studies were carried out by dissolving -10 mg of each new crystalline forms in water, gradually added, starting by 1 mL, and stirred until complete dissolution. The amount of water added, and the clarity of the solutions allowed the estimation of an empirical relative solubility behavior when compared to PZQ alone.

III. Results and Discussion

To follow the reaction progress, all the experimental attempts were firstly characterized by PXRD. Subsequently, depending on the successful results obtained by this technique, the experimental characterization was taken to further stages, namely SCRXD, HSM, DSC-TGA and FTIR-ATR. Lastly, with the aim of investigating potential changes in physicochemical properties, some stability and preliminary/ empirical solubility tests were performed.

When this work was proposed in March 2021, there were no cocrystals of PZQ and the coformers used reported in the literature, except for OXA. However, in May 2021, René de Gelder⁴⁸ and co-authors published their work where they predicted *“30 new coformer candidates for PZQ and their structural characterization and classification of 12 new cocrystalline forms of PZQ that were discovered”* with their approach⁴⁸. Turns out some of the coformers they predicted to be formed were the already being explored in this work: SAL, 4-ASA, 4-HBZ and VAN. Bearing these in mind, for these cocrystals, of the full data collection for structural elucidation from SCXRD was not carried out, and the CIFs deposited at CSD were used to describe the crystal structures.

1. Screening of new cocrystals of PZQ

In PZQ, only the oxygen atoms from the carbonyl groups function as hydrogen bond acceptors despite this drug having also in its structure two amide groups. This occurs due to the free electron pair of the N atoms involved in π -electron delocalization.

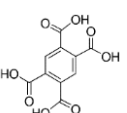
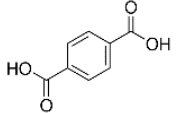
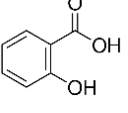
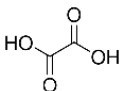
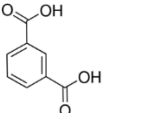
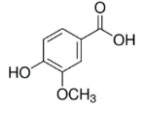
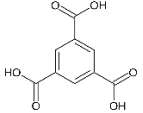
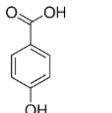
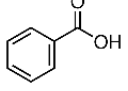
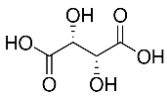
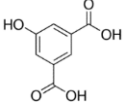
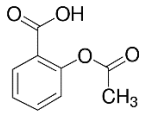
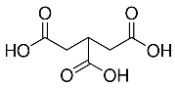
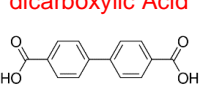
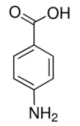
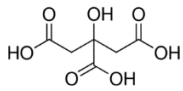
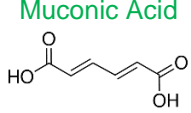
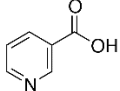
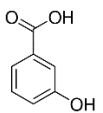
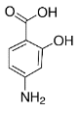
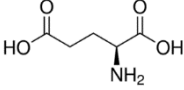
Considering the already reported cocrystals of PZQ by Herbert Höpfl⁴³, where the dominant hydrogen bonding patterns within the cocrystals were heterodimeric motifs formed O-H \cdots O hydrogen bonds between PZQ and dicarboxylic acids, all the coformers chosen for this work have at least one carboxylic acid in their structure. Some of them have also NH₂ groups, due to their capacity for acting as hydrogen bond donors. In addition, most of the coformers tested are GRAS by Food and Drug Administration (FDA).

After the synthetic procedure, in collaboration with Dra. Luisa Roca Paixão from the University of Lille, some computational studies were performed with the aim of comparing the experimental results with the predictions. Recurring to the COSMO-RS theory, these calculations were based on the affinity between PZQ and the coformers by using the excess (or mixing) enthalpy, ΔH_{ex} , of a virtual supercooled liquid of PZQ-coformer mixture relative to the pure components. This *“excess of enthalpy can be used as a parameter to evaluate the tendency of those compounds to form a cocrystal”*, being that the more negative this value, the more the compounds prefer the mixture with the regard to their pure state, and, therefore, higher probability of forming a cocrystal⁵⁶.

Analyzing the results of the simulations performed by Dra. Luisa Roca Paixão, presented in Table 6, it is possible to state that the majority of the coformers tested should had provided cocrystals with PZQ, yet some did not react under the tested synthetic conditions. Therefore, it would be good idea for future work to try to optimize the synthetic conditions to check if they provide cocrystals as predicted by the calculations.

It is important to note that all coformers that provided cocrystals present benzene rings, at least, disubstituted with carboxylic groups, except MUC that an aliphatic dicarboxylic acid.

Table 6 Computational calculations' results of the coformers tested that provided cocrystals (in green) and that did not provided cocrystals (in red) when combined with PZQ.

Coformer	ΔH_{ex}	Coformer	ΔH_{ex}	Coformer	ΔH_{ex}
1,2,4,5-Benzenetetracarboxylic Acid 	-7.93	Terephthalic Acid 	-3.84	Salicylic Acid 	-2.89
Oxalic Acid 	-6.27	Isophthalic Acid 	-3.75	Vanillic Acid 	-2.44
Trimesic Acid 	-5.62	4-Hydroxybenzoic Acid 	-3.67	Benzoic Acid 	-1.88
L-Tartaric Acid 	-5.52	5-Hydroxyisophthalic Acid 	-3.51	Aspirin 	-1.86
Tricarballic Acid 	-4.55	Biphenyl-4,4'-dicarboxylic Acid 	-3.23	4-Aminobenzoic Acid 	-1.86
Citric Acid 	-4.49	Trans,trans-Muconic Acid 	-3.16	Nicotinic Acid 	-0.89
3-Hydroxybenzoic Acid 	-3.96	4-Aminosalicylic Acid 	-2.92	L-Glutamic Acid 	0.06

In order to confirm the formation of new crystalline forms of (RS)-PZQ it is necessary to compare the PXRD patterns of the API, the respective coformer and the solid obtained from the LAG experiments. The presented PZQ and coformers simulated PXRD patterns were obtained from the CIF files of CSD with the entries TELCEU⁴³ (PZQ), SALIAC⁵⁷ (SAL), AMSALA02⁵⁸ (4-ASA), KEFGUA⁵⁹ (BTC),

CEHGUS⁶⁰ (VAN), BIDLOP02⁶¹ (3-HBZ), JOZZIH01⁶² (4-HBZ), BTCOAC⁶³ (TRI) and MUCONA⁶⁴ (MUC). 5-HIP was the exception in this process, being that its PXRD diffractogram was experimentally obtained.

In the first approach, the majority of the experiments generated new cocrystals with stoichiometric ratios of 1:1 and, for that reason, no other mechanochemical reactions with different stoichiometry were performed. In the cases where single crystals were provided, the proposed cocrystal composition was confirmed also by SCXRD analysis.

2. Structural characterization of PZQ new crystalline forms

2.1 PZQ·SAL

2.1.1 PXRD Analysis

The powder diffractograms for PZQ, SAL and the final product obtained by LAG are presented in Figure 4. The PXRD pattern for the 1:1 combination of PZQ and SAL showed a small peak of unreacted PZQ for a 2θ value of 4° . However, it is possible to affirm that the cocrystal obtained was formed through a stoichiometric composition of 1:1, which is confirmed by comparison with the PXRD pattern of the structure reported by René de Gelder⁴⁸. The shifts in the peak positions, especially for higher 2θ values are due to the difference of temperature used to obtain single crystal data (150 K) and the temperature used for the experimental PXRD pattern (RT).

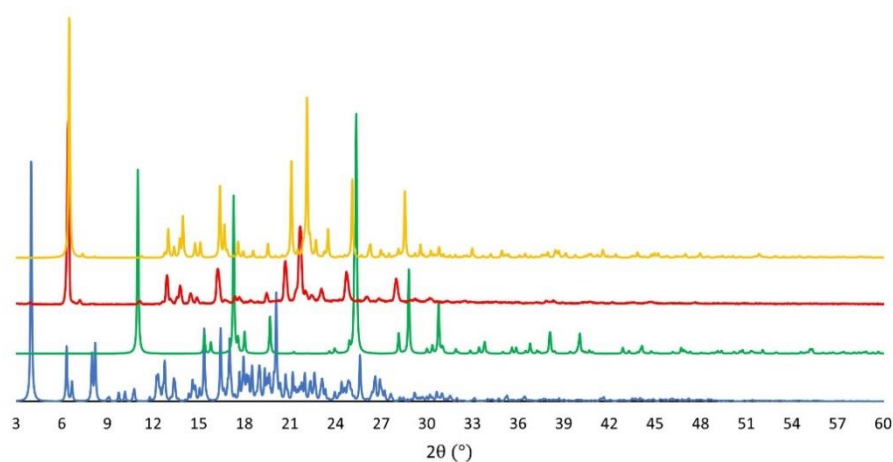


Figure 4 PXRD patterns for the following samples: PZQ (in blue), SAL (in green), PZQ·SAL prepared by LAG with acetonitrile with 1:1 stoichiometry (in red), and the pattern of PZQ·SAL simulated from the literature (in yellow).

2.1.2 SCXRD Analysis

This crystalline form provided single crystals suitable for SCXRD. However, during the indexing process it was noticed that the unit cell parameters and the space group of the cocrystal (crystallographic data in Table S1) matched the structure reported by René de Gelder⁴⁸, which is represented in Figure 5, confirming the reproduction of this form. The asymmetric unit of PZQ·SAL consists of one molecule of

PZQ, one of SAL and one of water. Both intermolecular and intramolecular H-bonds in this cocrystal are presented in Figure 5a, evidencing the $R_4^2(8)$ synthons formed between the carbonyls of PZQ and the water molecules. The intermolecular H-bonds form $D_1^1(2)$ synthons that are established between the O-H_{COOH} (from the coformer) and the carbonyl of the amide group (from PZQ) ($O_3-H_2\cdots O_4$ 2.564(2) Å); the other carbonyl from PZQ bonds to the O-H_{H₂O} ($O_6-H_{31}\cdots O_5$ 2.832(3) Å and $O_6-H_{32}\cdots O_5$ 2.838(3) Å). The intramolecular H-bonds between O-H_{OH} and the carbonyl of SAL ($O_2-H_1\cdots O_1$ 2.598(2) Å) are maintained in the cocrystal hydrate, forming the $S_1^1(6)$ synthon. The supramolecular crystal packing is presented in Figure 5b, showing that in the cocrystal hydrate two molecules of PZQ bridge via two water molecules⁴⁸. Hydrogen bond details for PZQ·SAL are given in Table 7.

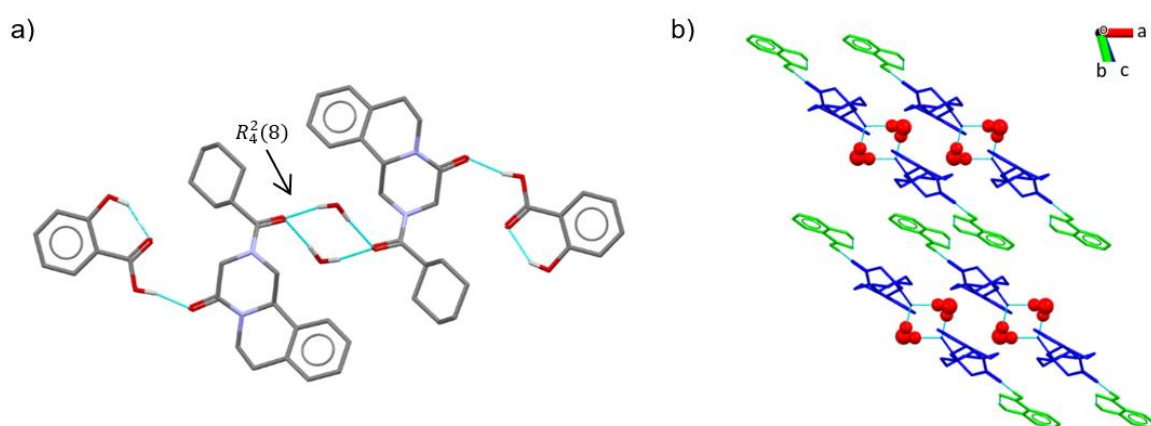


Figure 5 Intramolecular and intermolecular hydrogen bonds in PZQ·SAL cocrystal hydrate; (b) supramolecular crystal packing (view along c^* axis) of PZQ molecules (in blue), SAL (in green) and water (in red). All non-contact H atoms were omitted for clarity.

Table 7 List of the main hydrogen bonds found for PZQ·SAL cocrystal hydrate.

Sym. Op.	D-H...A	$d(D-H)$ (Å)	$d(H\cdots A)$ (Å)	$d(D\cdots A)$ (Å)	(DHA) (°)
x, y, z	$O_2-H_1\cdots O_1$	0.84	1.86	2.598(2)	146
$x, y, -1+z$	$O_3-H_2\cdots O_4$	0.84	1.74	2.564(2)	166
$x, y, -1+z$	$O_6-H_{31}\cdots O_5$	0.87(3)	1.97(2)	2.832(3)	169(4)
$-x, -y, 1-z$	$O_6-H_{32}\cdots O_5$	0.87(3)	1.98(4)	2.838(3)	172(3)

2.1.3 IR Spectroscopy

Comparing the solid-state IR spectra of PZQ, the cocrystal former and the corresponding cocrystal allows to confirm if a new solid form was generated during the mechanochemical process. This is illustrated in Figure 6, showing that the IR spectrum of the cocrystal do not correspond to a superposition of the IR spectra of the two reagents. Since PZQ has two amide groups in its structure, it is expected to observe the amide band corresponding to the carbonyl stretching vibrations of the amide groups in the cocrystal IR spectra, which is observed at 1592 and 1577 cm^{-1} . SAL has one carboxylic acid group and, therefore, the carbonyl stretching vibration derived from this group is represented at 1670 cm^{-1} , as well

as a broad band at 3531-3461 cm^{-1} derived from the OH stretch involved in intermolecular and intramolecular H-bonding. The list of relevant IR bands for the new cocrystals is presented in Table S2. The shifts in the cocrystal spectra in comparison to the values observed for these functional groups in PZQ and SAL indicate variations in the H-bonding pattern within the crystal structure of the resulting cocrystal. Also, when the cocrystal is formed, higher energies (higher wavenumbers) are required for the carbonyl stretching⁴³. This assignment confirms the cocrystal hydrate structure presented in Figure 5a.

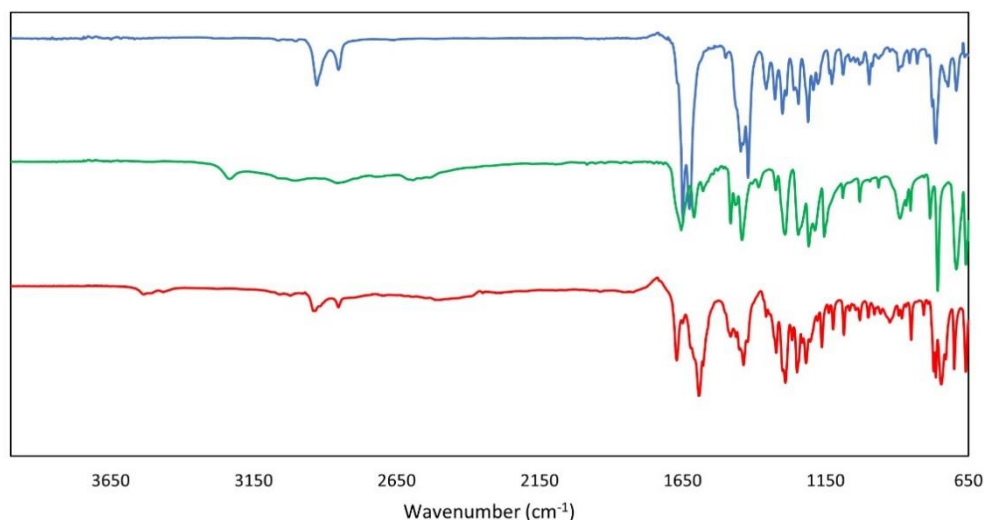


Figure 6 FTIR-ATR spectra of PZQ (in blue), SAL (in green) and PZQ·SAL (in red).

2.1.4 DSC-TGA and HSM

According to the DSC-TGA trace, presented in Figure 7a, it is possible to state that the PZQ·SAL cocrystal melts approximately at 90.25 °C, event represented by the endothermic peak with no significant mass loss. However, and since this cocrystal is in its hydrate form, it would be expected to observe in the TGA a 3.84 % mass loss around 100 °C, corresponding to the loss of the water molecule. In addition, it can be affirmed that decomposition starts at 218 °C due to the endothermic peak after melting with gradual mass loss. The HSM images (Figure 7b) are in good agreement with this assumption despite the temperature presented for melting being slightly higher for this technique. Such happens because the cover glass of the HSM was open during the experiment to allow better visualization of the crystals, making the actual temperature lower than the recorded one.

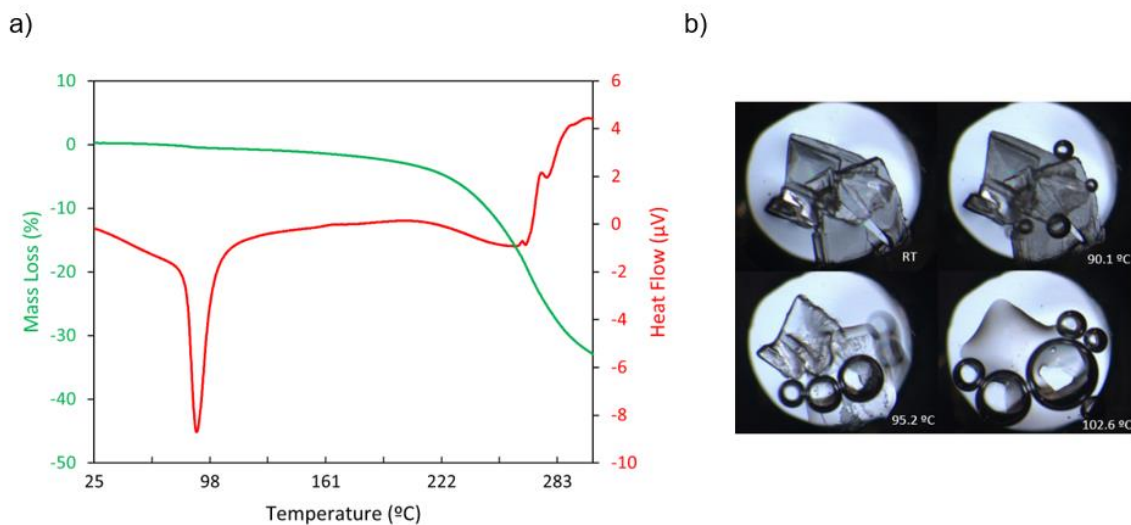


Figure 7 (a) DSC (in red) - TGA (in green) and (b) HSM images for PZQ·SAL.

2.2 PZQ·4-ASA

2.2.1 PXRD Analysis

The diffractograms for PZQ, 4-ASA and the reacted product by LAG are presented in Figure 8. The pattern for the 1:1 combination of PZQ and 4-ASA does not contain peaks of residual starting materials, suggesting the formation of a 1:1 cocrystal for PZQ·4-ASA. In addition, the PXRD pattern simulated from literature confirms this hypothesis⁴⁸. As in the PZQ·SAL case, it is possible to observe a small shift of the powder analysis in relation to the simulated powder due to the different temperatures of the data collections.

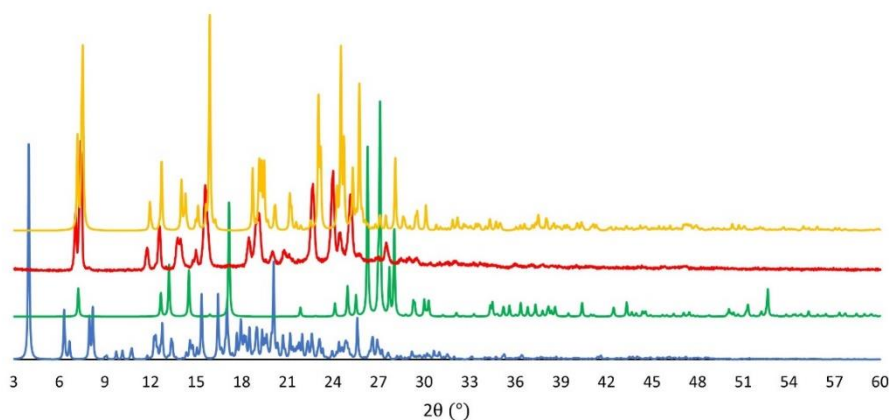


Figure 8 PXRD patterns for the following samples: PZQ (in blue), 4-ASA (in green), PZQ·4-ASA prepared by LAG with acetonitrile with 1:1 stoichiometry (in red), and the pattern of PZQ·4-ASA simulated from the literature (in yellow).

2.2.2 SCXRD Analysis

As the PZQ·SAL case, PZQ·4-ASA provided single-crystals suitable for SCXRD similar to the ones already reported by René de Gelder⁴⁸ (crystallographic data in Table S1). In Figure 9, it is represented the structure of this cocrystal solvate. The asymmetric unit of PZQ·4-ASA consists of one molecule of PZQ, one of 4-ASA and one of acetonitrile. Both intermolecular and intramolecular H-bonds in this cocrystal are presented in Figure 9a. The intermolecular H-bonds form the $D_1^1(2)$ synthons that are established between the O–H_{COOH} (from the coformer) and the carbonyl of the amide group (from PZQ) ($O_3-H_{25} \cdots O_1$ 2.643(2) Å); one of the N–H_{NH2} from 4-ASA bonds to NC of acetonitrile, creating the synthon $D_1^1(2)$, ($N_3-H_{27} \cdots N_4$ 3.149(3) Å) while the other N–H_{NH2} bonds to the carbonyl of PZQ ($N_3-H_{28} \cdots O_2$ 2.8567(18) Å). The intramolecular H-bonds between the hydroxyl and the carbonyl of 4-ASA are maintained in the cocrystal solvate ($O_5-H_{26} \cdots O_4$ 2.584(2) Å), forming the $S_1^1(6)$ synthon. The supramolecular crystal packing is presented in Figure 9b, showing the formation of layers with complementary chains. Hydrogen bond details for PZQ·4-ASA are given in Table 8.

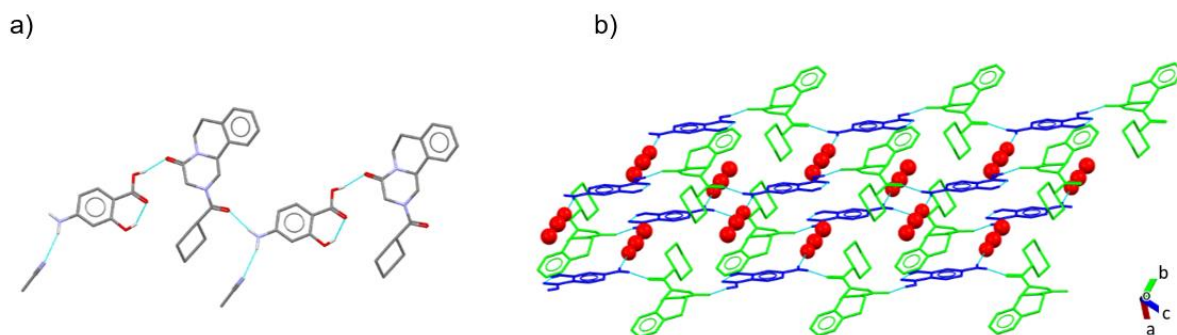


Figure 9 (a) Intramolecular and intermolecular hydrogen bonds in PZQ·4-ASA cocrystal solvate; (b) supramolecular crystal packing of PZQ molecules (in green), 4-ASA (in blue) and acetonitrile (in red). All non-contact H atoms were omitted for clarity.

Table 8 List of the main hydrogen bonds found for PZQ·4-ASA cocrystal solvate.

Sym. Op.	D–H...A	<i>d</i> (D–H) (Å)	<i>d</i> (H...A) (Å)	<i>d</i> (D...A) (Å)	(DHA) (°)
<i>x, y, z</i>	$O_3-H_{25} \cdots O_1$	0.84	1.82	2.643(2)	164
<i>x, y, z</i>	$O_5-H_{26} \cdots O_4$	0.84	1.84	2.584(2)	147
<i>x, y, z</i>	$N_3-H_{27} \cdots N_4$	0.88	2.33	3.149(3)	155
$-1+x, -1+y, -1+z$	$N_3-H_{28} \cdots O_2$	0.88	1.99	2.8567(18)	169

2.2.3 IR Spectroscopy

The FTIR-ATR spectrum of PZQ·4-ASA and its reagents are presented in Figure 10, confirming that a new cocrystal is formed by the not superposition with the reagent's spectra. The peaks at 1635 and 1610 cm⁻¹ can be attributed to carbonyl stretching vibrations of the amide groups while the peaks at 3444 and 3336 cm⁻¹ are related to the NH stretch of the aromatic primary amine present in 4-ASA. The

peak at 2252 cm^{-1} represents the aliphatic nitrile of acetonitrile. Also, the intermolecular and intramolecular H-bonding are represented by broad 3232 cm^{-1} peak (Table S2). This assignment confirms the cocrystal solvate structure presented in Figure 9a.

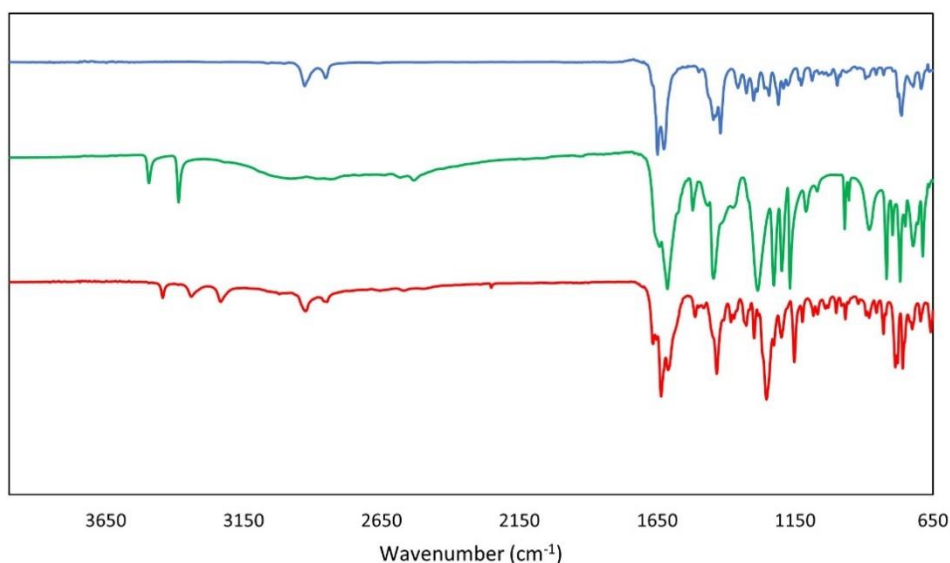


Figure 10 FTIR-ATR spectra of PZQ (in blue), 4-ASA (in green) and PZQ·4-ASA (in red).

2.2.4 DSC-TGA

In the DSC-TGA trace, presented in Figure 11, it is possible to observe a phase transition, with a mass loss of 4.5 %, that was detected at $T_{max} = 96.6\text{ }^{\circ}\text{C}$, as well as a second event ($T_{on} = 137\text{ }^{\circ}\text{C}$, $T_{max} = 160.3\text{ }^{\circ}\text{C}$). The first phenomenon was attributed to the release of the molecule of acetonitrile present in the cocrystal solvate structure, corresponding to the percentage of mass loss (8.1 % vs 4.5 %), while the second involves the melting of the cocrystal. Unfortunately, it was not possible to perform some HSM experiments to confirm this assignment.

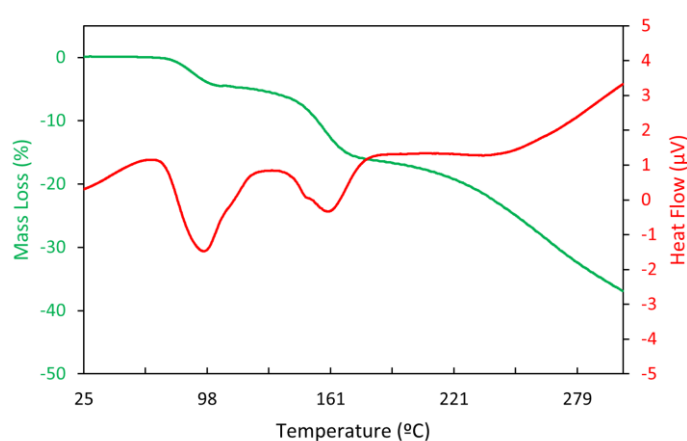


Figure 11 DSC (in red) -TGA (in green) of PZQ·4-ASA.

2.3 PZQ·BTC 2:1

2.3.1 PXRD Analysis

The powder diffractograms for PZQ, BTC and the final product obtained by LAG are presented in Figure 12. The diffractogram of the bulk resulting from the grinding experiment does not contain peaks of residual starting materials, suggesting the formation of cocrystals for PZQ·BTC. Despite having started from a 1:1 stoichiometric composition, the SCXRD data suggested the formation of 2:1 cocrystals. The synthetic conditions were optimized for 2:1 ratio, whose PXRD pattern was in good agreement with the simulated from the single crystal data, confirming the hypothesis that PZQ and BTC provide cocrystals with a 2:1 stoichiometric composition.

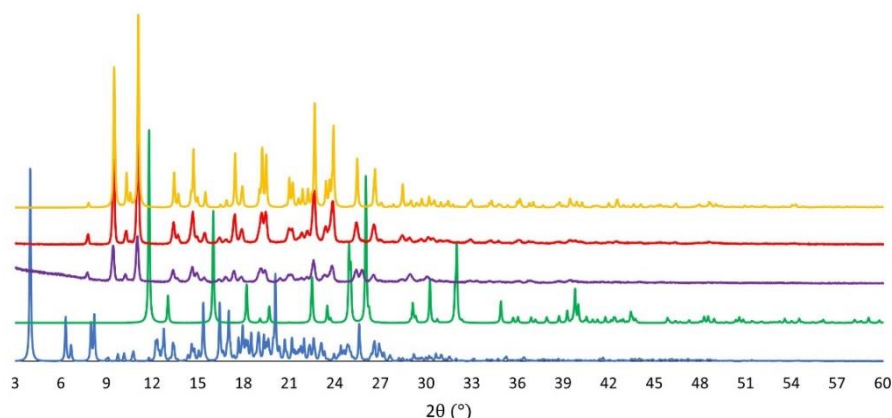


Figure 12 PXRD patterns for the following samples: PZQ (in blue), BTC (in green), PZQ·BTC prepared by LAG with acetonitrile with 1:1 stoichiometry (in purple), PZQ·BTC prepared by LAG with acetonitrile with 2:1 stoichiometry (in red) and the pattern of PZQ·BTC 2:1 simulated from the SCXRD analysis (in yellow).

2.3.2 SCXRD Analysis

Since this new form provided single crystals that were not reported yet, the crystal structure elucidation was performed from SCXRD data. The illustration of intermolecular interactions and the crystal packing of PZQ·BTC 2:1 is presented in Figure 13. The asymmetric unit of PZQ·BTC 2:1 consists of two molecules of PZQ and one of BTC. Both intermolecular H-bonds, in Figure 13a, are established between the O-H_{COOH} (from the coformer) and the carbonyl of the amide group (from PZQ) (O₃-H₃...O₂ 2.626(4) Å and O₆-H₆...O₁ 2.940(10) Å), forming $D_1^1(2)$ synthons. The supramolecular crystal packing is presented in Figure 13b, evidencing the $R_4^4(28)$ synthons formed between the carboxylic moieties of BTC and the C=O from PZQ. BTC has four carboxylic groups in its structure, being that each of these moieties bonds to one molecule of API. The packing of this cocrystal is shaped through parallel plates of molecules bonded by the $R_4^4(28)$ synthons. Hydrogen bond details for PZQ·BTC 2:1 are given in Table 9.

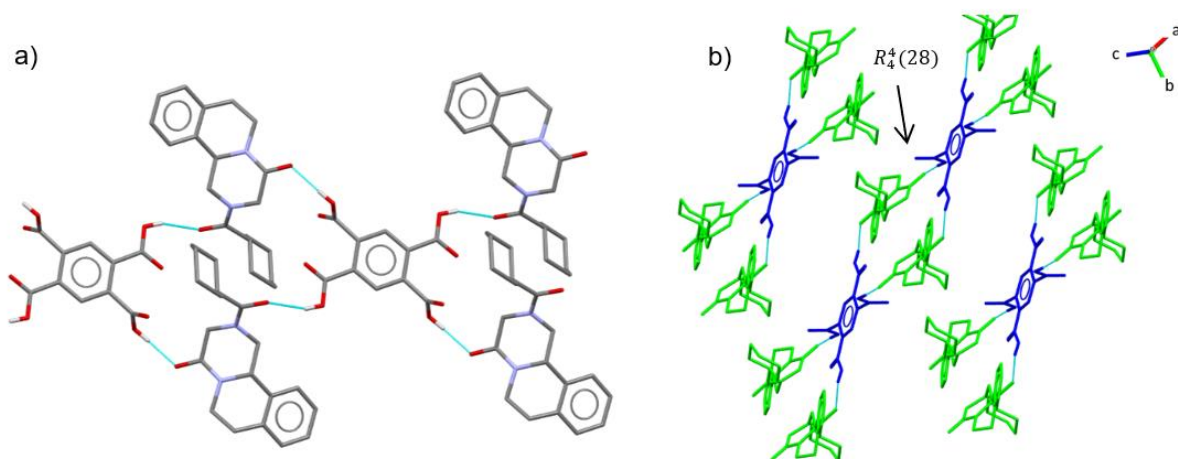


Figure 13 a) Intramolecular and intermolecular hydrogen bonds in PZQ·BTC 2:1 cocrystal; (b) supramolecular crystal packing of PZQ molecules (in green) and BTC (in blue). All non-contact H atoms were omitted for clarity.

Table 9 List of the main hydrogen bonds found for compound PZQ·BTC 2:1.

Sym. Op.	D–H...A	<i>d</i> (D–H) (Å)	<i>d</i> (H...A) (Å)	<i>d</i> (D...A) (Å)	(DHA) (°)
<i>x, y, z</i>	O ₃ –H ₃ ...O ₂	0.82	1.81	2.626(4)	173
<i>1-x, 1-y, 1-z</i>	O ₆ –H ₆ ...O ₁	0.82	2.17	2.940(10)	156

2.3.3 IR Spectroscopy

In Figure 14, it is presented the FTIR-ATR spectrum of PZQ·BTC 2:1 and its reagents. The not superposition of the spectra of the two reagents with the final product confirms the formation of a new cocrystal. The peaks at 1592 and 1585 cm⁻¹ can be attributed to the carbonyl stretching vibrations of the amide groups while the peak at 1708 cm⁻¹ is related to the carbonyl stretching vibration caused by the carboxylic group of the coformer. Also, the intermolecular and intramolecular H-bonding are represented by broad band at 3021-2852 cm⁻¹ (Table S2). This assignment is in good agreement with the cocrystal structure presented previously in Figure 13.

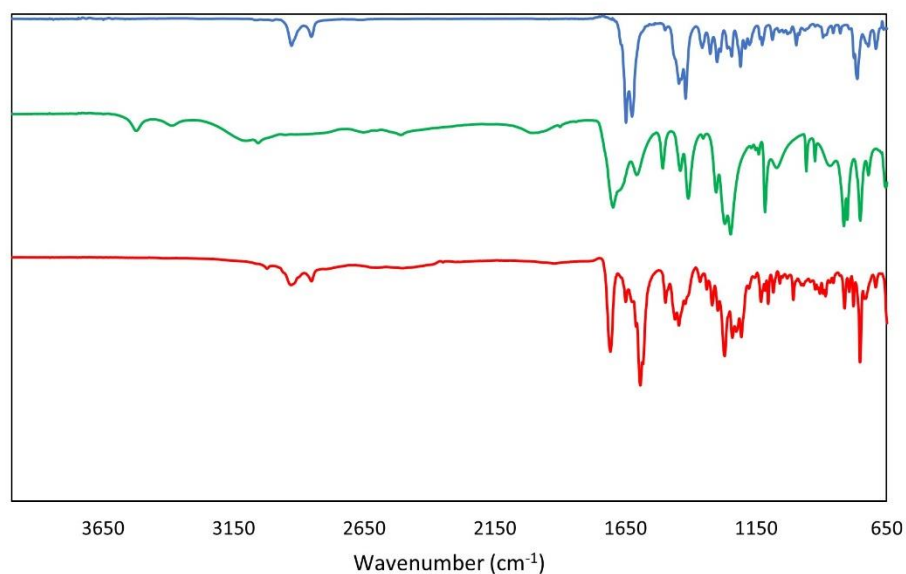


Figure 14 FTIR-ATR spectra of PZQ (in blue), BTC (in green) and PZQ·BTC 2:1 (in red).

2.3.4 DSC-TGA and HSM

According to the results presented in Figure 15a, it is possible to see that the melting and decomposition of PZQ·BTC 2:1 starts at 182 °C with a T_{max} = 210,13 °C. Also, this assignment can be corroborated by the HSM images (Figure 15b) despite the temperature presented for melting being slightly higher for this technique.

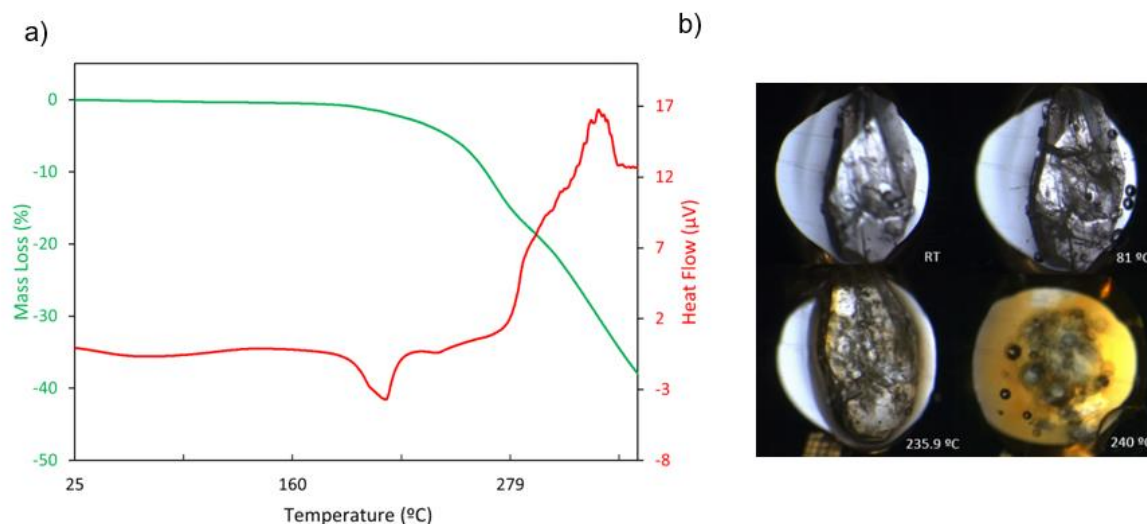


Figure 15 (a) DSC (in red) – TGA (in green) and (b) HSM images for PZQ·BTC 2:1.

2.4 PZQ·VAN

2.4.1 PXRD Analysis

In Figure 16 it is presented the diffractograms for the cocrystal PZQ·VAN obtained by LAG and its reagents. The diffraction pattern for the 1:1 combination of PZQ and VAN does not contain peaks of residual starting materials, suggesting the formation of a 1:1 cocrystal for PZQ·VAN. In addition, the PXRD pattern simulated from the literature is in good agreement with the experimentally observed diffractogram of the 1:1 crystalline powder⁴⁸. The differences in the experimental (RT) and the simulated pattern (150 K) are derived from the difference of temperature in the experiment's measurement.

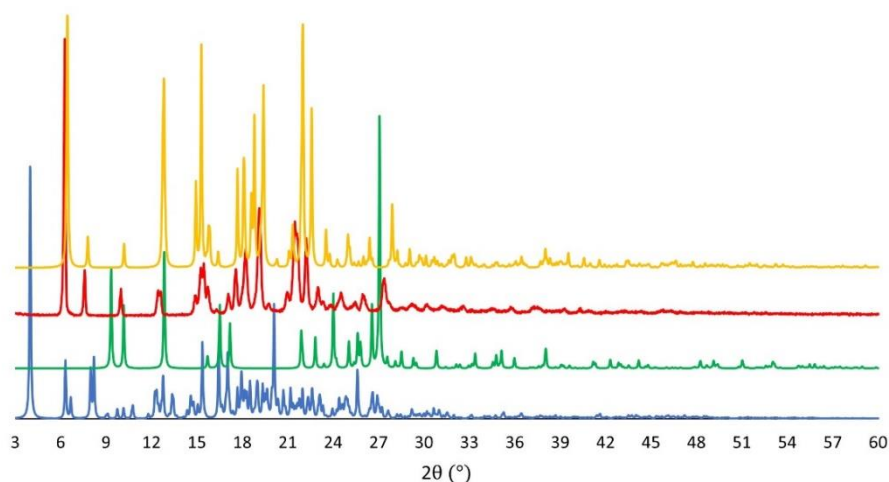


Figure 16 PXRD patterns for the following samples: PZQ (in blue), VAN (in green), PZQ·VAN prepared by LAG with acetonitrile with 1:1 stoichiometry (in red), and the pattern of PZQ·VAN simulated from the literature (in yellow).

2.4.2 SCXRD Analysis

PZQ·VAN also provided single-crystals suitable for SCXRD that were similar to the ones already reported by René de Gelder⁴⁸ (crystallographic data in Table S1). In Figure 17 is represented the structure of this cocrystal. The asymmetric unit of PZQ·VAN consists of one molecule of PZQ and one of VAN. The intermolecular H-bonds in this cocrystal are presented in Figure 17a, evidencing the $R_2^2(8)$ synthons formed between the carboxylic moieties of VAN. These H-bonds are established between the O-H_{COOH} from VAN bonds to the C=O_{COOH} of another VAN molecule while the C=O_{COOH} bonds to O-H_{COOH} of the first VAN molecule ($O_5-H_{37} \cdots O_6$ 2.6080(13) Å); the hydroxyl (from the coformer) also bonds the carbonyl of the amide group (from PZQ) ($O_3-H_{36} \cdots O_1$ 2.6534(10) Å), forming the $D_1^1(2)$ synthon. The intramolecular H-bonds between the hydroxyl and the O-C_{COCH}3 of VAN are maintained in the cocrystal ($O_3-H_{36} \cdots O_4$ 2.7024(11) Å) despite not being represented in the figure. The supramolecular crystal

packing is presented in Figure 17b, showing the formation of zigzag chains. Hydrogen bond details for PZQ·VAN are given in Table 10.

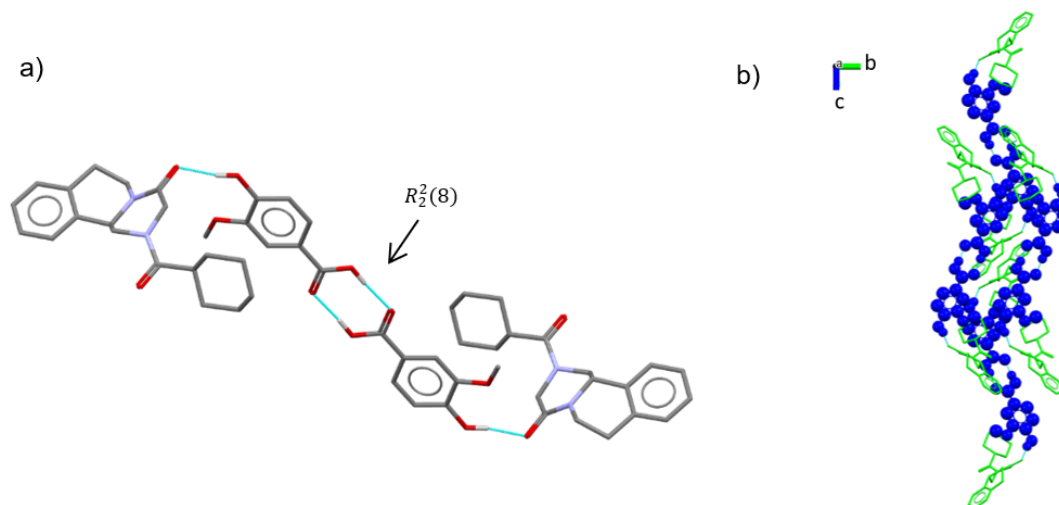


Figure 17 (a) Intermolecular hydrogen bonds in PZQ·VAN cocrystal; (b) supramolecular crystal packing (view along *a* axis) of PZQ molecules (in green) and VAN (in blue). All non-contact H atoms were omitted for clarity.

Table 10 List of the main hydrogen bonds found for compound PZQ·VAN.

Sym. Op.	D–H...A	<i>d</i> (D–H) (Å)	<i>d</i> (H...A) (Å)	<i>d</i> (D...A) (Å)	(DHA) (°)
<i>x, y, z</i>	O ₃ –H ₃₆ ...O ₁	0.921(17)	1.755(16)	2.6534(10)	164.4(16)
<i>x, y, z</i>	O ₃ –H ₃₆ ...O ₄	0.921(17)	2.322(18)	2.7024(11)	104.4(12)
<i>1-x, 1-y, 2-z</i>	O ₅ –H ₃₇ ...O ₆	0.87(4)	1.74(4)	2.6080(13)	176(3)
<i>1-x, 1-y, 2-z</i>	O ₆ –H ₄₄ ...O ₅	0.88(7)	1.73(7)	2.6080(13)	175(5)

2.4.3 IR Spectroscopy

In Figure 18 it is presented the FTIR-ATR spectrum of the two cocrystal formers and PZQ·VAN, showing that the reagents peaks differ from the cocrystal spectra. The peak at 1637 cm⁻¹ can be attributed to carbonyl stretching vibrations of the amide group while the peak at 1672 cm⁻¹ is related to the carbonyl stretching vibration caused by the carboxylic group of the coformer. Also, the intermolecular and intramolecular H-bonding are represented by broad band at 3004-2840 cm⁻¹ (Table S2). The cocrystal structure presented previously in Figure 17a is confirmed by these peaks' attributions.

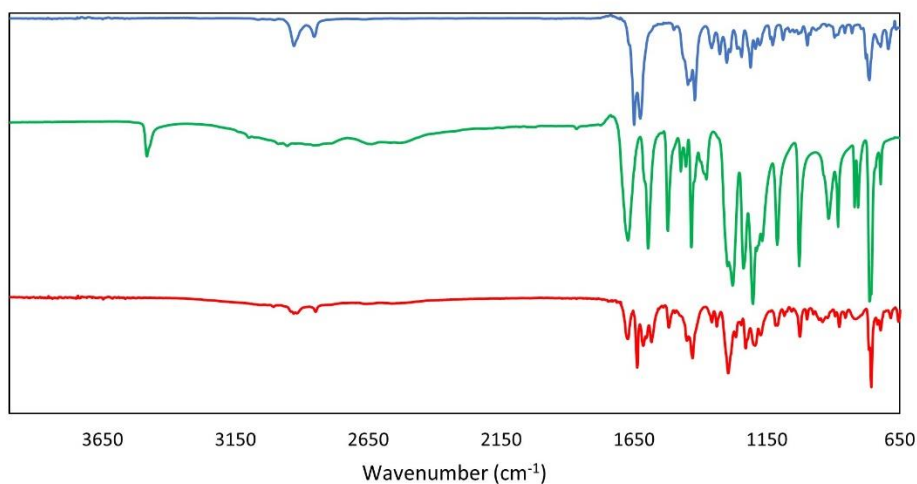


Figure 18 FTIR-ATR spectra of PZQ (in blue), VAN (in green) and PZQ·VAN (in red).

2.4.4 DSC-TGA and HSM

According to the DSC-TGA trace, presented in Figure 19a, it is possible to state that the PZQ·VAN cocrystal starts to melt at 130 °C with $T_{max} = 137.3$ °C and, since there is no mass loss detected around 100 °C, is confirmed that this cocrystal is an anhydrous form. In addition, it can be stated that decomposition starts at 215 °C due to the gradual mass loss. The HSM images (Figure 19b) corroborate DSC-TGA data.

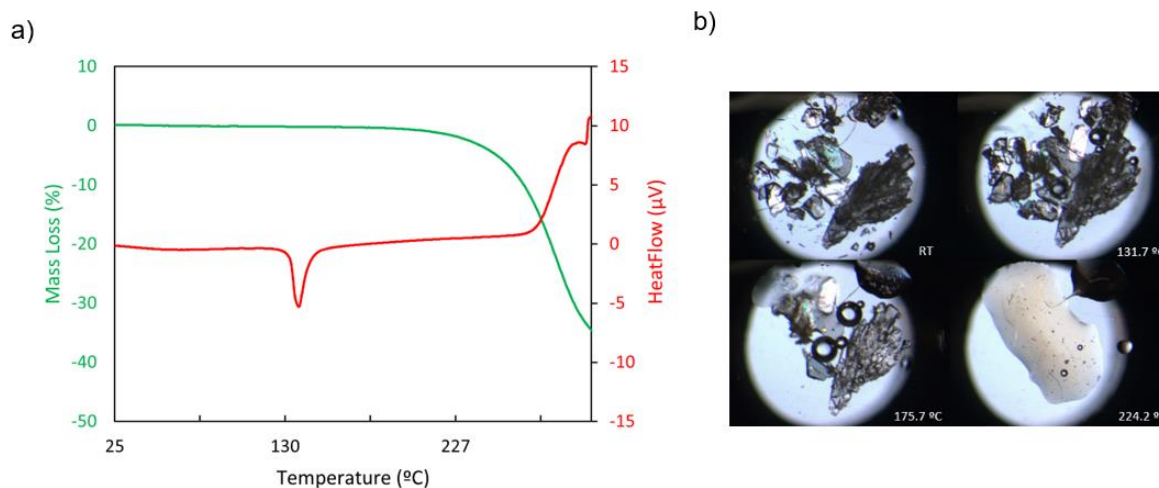


Figure 19 (a) DSC (in red) – TGA (in green) and (b) HSM imagens for PZQ·VAN.

2.5 PZQ·3-HBZ 2:1

2.5.1 PXRD Analysis

In Figure 20 is presented the PXRD diffractograms for PZQ, 3-HBZ and the final product obtained by LAG. The grinding experiment was performed starting from a 1:1 stoichiometric ratio although the SCXRD data suggested the formation of cocrystals in a stoichiometry of 2:1. Therefore, the mechanochemical reaction' conditions were optimized for the 2:1 ratio. Despite the 1:1 compound proving also a new cocrystal, this was only characterized by PXRD. The structural elucidation was performed for the 2:1 cocrystals since its PXRD diffractogram was in good agreement with the single crystals provided.

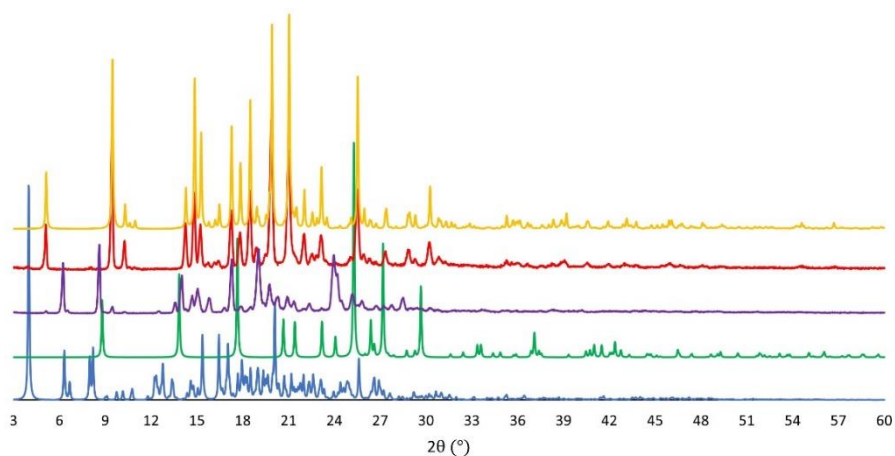


Figure 20 PXRD patterns for the following samples: PZQ (in blue), 3-HBZ (in green), PZQ·3-HBZ prepared by LAG with acetone with 1:1 stoichiometry (in purple), PZQ·3-HBZ prepared by LAG with acetone with 2:1 stoichiometry (in red) and the pattern of PZQ·3-HBZ 2:1.

2.5.2 SCXRD Analysis

Since this new form provided single crystals that were not reported yet, the crystal structure elucidation was also performed. The illustration of intermolecular interactions, and the crystal packing of PZQ·3-HBZ 2:1 is presented in Figure 21. The asymmetric unit of PZQ·3-HBZ 2:1 consists of two molecules of PZQ and one of 3-HBZ. The intermolecular H-bonds in this cocrystal are presented in Figure 21a. The intermolecular H-bonds evidence the formation of $D_1^1(2)$ synthons that are established between the O-H_{COOH} (from the coformer) and the carbonyl of the amide group (from PZQ) ($O_6-H_2 \cdots O_1$ 2.689(8) Å); another H-bond is formed between the hydroxyl group of 3-HBZ and the carbonyl of the second molecule of PZQ ($O_7-H_{20} \cdots O_4$ 2.657(8) Å). The crystal packing is presented in Figure 21b, showing that supramolecular arrangement forms diagonal parallel lines of 3-HBZ bonded to two molecules of PZQ. Hydrogen bond details for PZQ·3-HBZ 2:1 are given in Table 11.

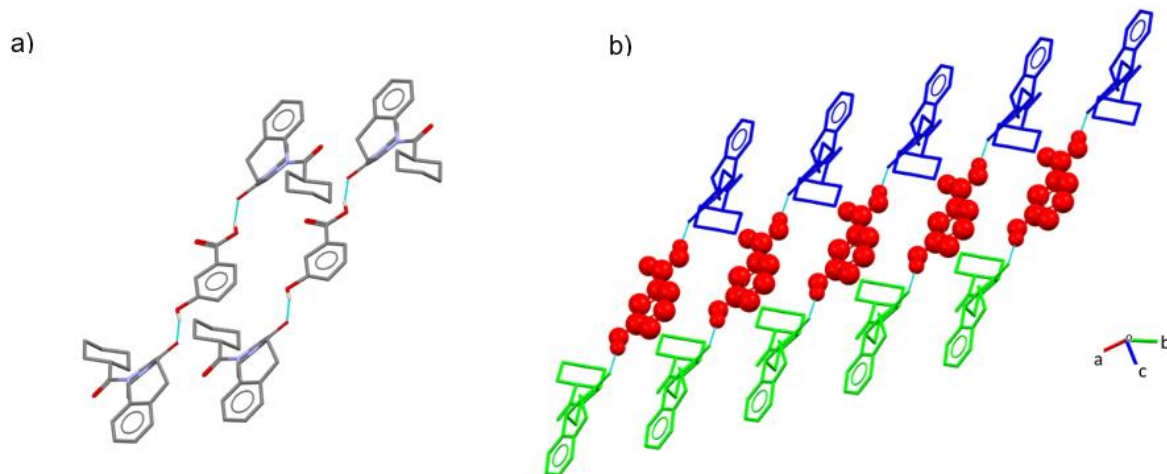


Figure 21 (a) Intermolecular hydrogen bonds in PZQ·3-HBZ 2:1 cocrystal; (b) supramolecular crystal packing of PZQ molecules (in green and blue) and 3-HBZ (in red). All non-contact H atoms were omitted for clarity.

Table 11 List of the main hydrogen bonds found for compound PZQ·3-HBZ 2:1.

Sym. Op.	D–H...A	$d(\text{D–H})$ (Å)	$d(\text{H...A})$ (Å)	$d(\text{D...A})$ (Å)	(DHA) (°)
x, y, z	$\text{O}_6\text{--H}_2\cdots\text{O}_1$	0.82	1.88	2.689(8)	167
x, y, z	$\text{O}_7\text{--H}_{20}\cdots\text{O}_4$	0.82	1.85	2.657(8)	167

2.5.3 IR Spectroscopy

The FTIR-ATR spectrum of PZQ·3-HBZ 2:1 and its reagents are presented in Figure 22, confirming the formation of the cocrystal since the spectra of the reagents do not overlap with the cocrystal spectra. The peaks at 1631 and 1612 cm^{-1} can be attributed to carbonyl stretching vibrations of the amide groups while the peak at 1714 cm^{-1} is related to the carbonyl stretching vibration caused by the carboxylic group of the coformer (Table S2). The cocrystal structure presented in Figure 21a is in good agreement with assignment.

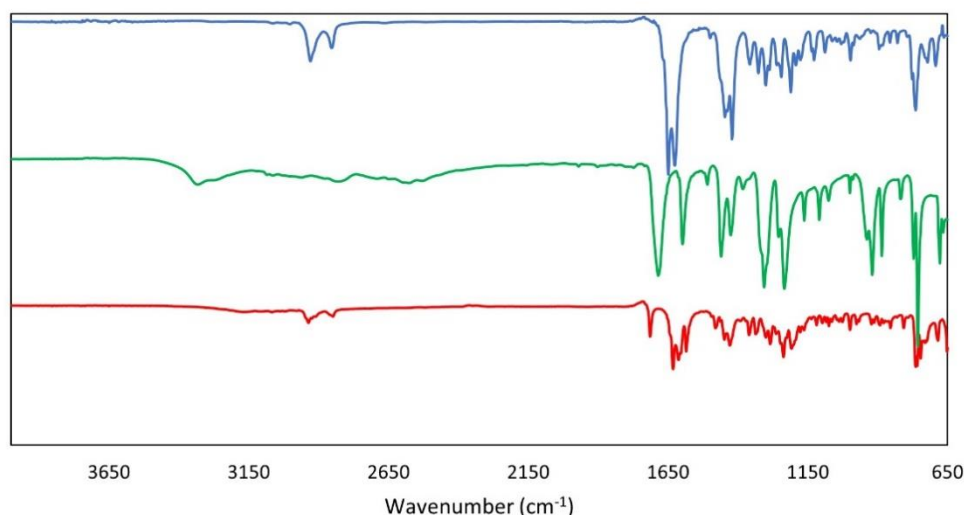


Figure 22 FTIR-ATR spectra for PZQ (in blue), 3-HBZ (in green) and PZQ·3-HBZ 2:1 (in red).

2.5.4 DSC-TGA and HSM

According to the DSC-TGA trace, presented in Figure 23a, it is possible to state that the PZQ·3-HBZ 2:1 cocrystal starts to melt at 94 °C with $T_{max} = 105$ °C and, since there is no mass loss detected around 100 °C, it is confirmed that this cocrystal is an anhydrous form. Decomposition starts at 230 °C, being evidenced by the endothermic peak complemented by gradual mass loss. As in PZQ·VAN, the HSM images (Figure 23b) are in good agreement with this assumption despite the temperature presented for melting being higher for this technique.

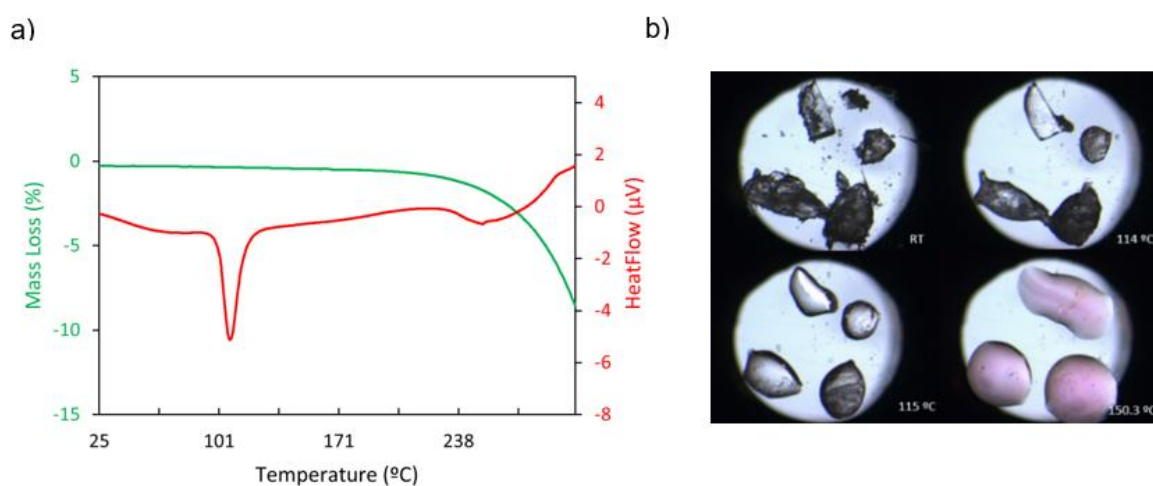


Figure 23 (a) DSC (in red) – TGA (in green) and (b) HSM images for PZQ·3-HBZ 2:1.

2.6 PZQ·4-HBZ

2.6.1 PXRD Analysis

The diffractograms for PZQ, 4-HBZ and PZQ·4-HBZ cocrystal obtained by LAG are presented in Figure 24. The pattern for the 1:1 combination of PZQ and 4-HBZ does not contain peaks of residual starting materials, suggesting the formation of a 1:1 cocrystal for PZQ·4-HBZ. Also, the PXRD pattern simulated from the structure deposited in CDS by de Gelder confirms this theory⁴⁸. Once again, the experimental (RT) and the simulated (150 K) PXRD patterns do not match exactly due to the difference of temperature of data acquisition.

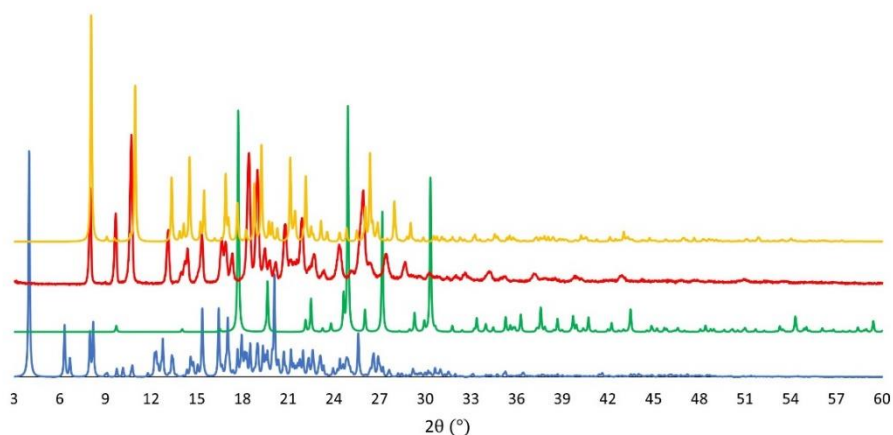


Figure 24 PXRD patterns for the following samples: PZQ (in blue), 4-HBZ (in green), PZQ·4-HBZ prepared by LAG with acetonitrile with 1:1 stoichiometry (in red), and the pattern of PZQ·4-HBZ simulated from the literature (in yellow).

2.6.2 SCXRD Analysis

PZQ·4-HBZ provided single-crystals suitable for SCXRD that were similar to the already reported by René de Gelder⁴⁸ (crystallographic data in Table S1). In Figure 25 is represented the structure of this cocrystal. The asymmetric unit of PZQ·4-HBZ consists of one molecule of PZQ and one of 4-HBZ. The intermolecular H-bonds in this cocrystal are presented in Figure 25a. The intermolecular H-bonds form $D_1^1(2)$ synthons that are established between the O-H_{COOH} (from the coformer) and the carbonyl of the amide group (from PZQ) ($O_4-H_{28} \cdots O_1$ 2.6798(8) Å); another H-bond is formed between the hydroxyl group of 4-HBZ and the other carbonyl of PZQ ($O_5-H_{29} \cdots O_2$ 2.6993(12) Å). The supramolecular crystal packing is presented in Figure 25b, showing that the molecules are organized in complementary chains with the coformer regarded as interchangeable agents for cocrystal formation⁴⁸. Hydrogen bond details for PZQ·4-HBZ are given in Table 12.

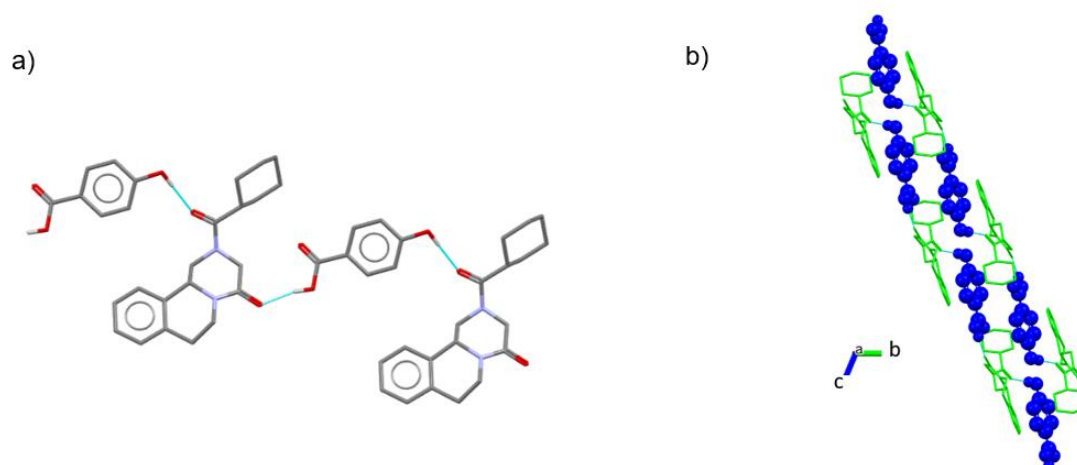


Figure 25 (a) Intermolecular hydrogen bonds in PZQ-4-HBZ cocrystal; (b) supramolecular crystal packing (view along a axis) of PZQ molecules (in green) and 4-HBZ (in blue). All non-contact H atoms were omitted for clarity.

Table 12 List of the main hydrogen bonds found for compound PZQ-4-HBZ.

Sym. Op.	D–H...A	<i>d</i> (D–H) (Å)	<i>d</i> (H...A) (Å)	<i>d</i> (D...A) (Å)	(DHA) (°)
$-1+x, -1+y, -1+z$	O ₄ –H ₂₈ ...O ₁	0.881(15)	1.816(16)	2.6798(8)	166.2(16)
x, y, z	O ₅ –H ₂₉ ...O ₂	0.853(18)	1.849(18)	2.6993(12)	174.8(18)
x, y, z	O ₅ –H ₂₉ ...O ₃	0.853(18)	1.68(2)	2.513(17)	165.3(17)

2.6.3 IR Spectroscopy

In Figure 26 is presented the IR spectrum of PZQ-4-HBZ and its reagents. The peak at 1618 and 1591 cm^{-1} can be attributed to carbonyl stretching vibrations of the amide groups while the peak at 1704 cm^{-1} is related to the carbonyl stretching vibration caused by the carboxylic group of the coformer. Also, the intermolecular and intramolecular H-bonding are represented by broad band at 3209 cm^{-1} (Table S2). This assignment can be confirmed by the cocrystal structure already presented in Figure 25.

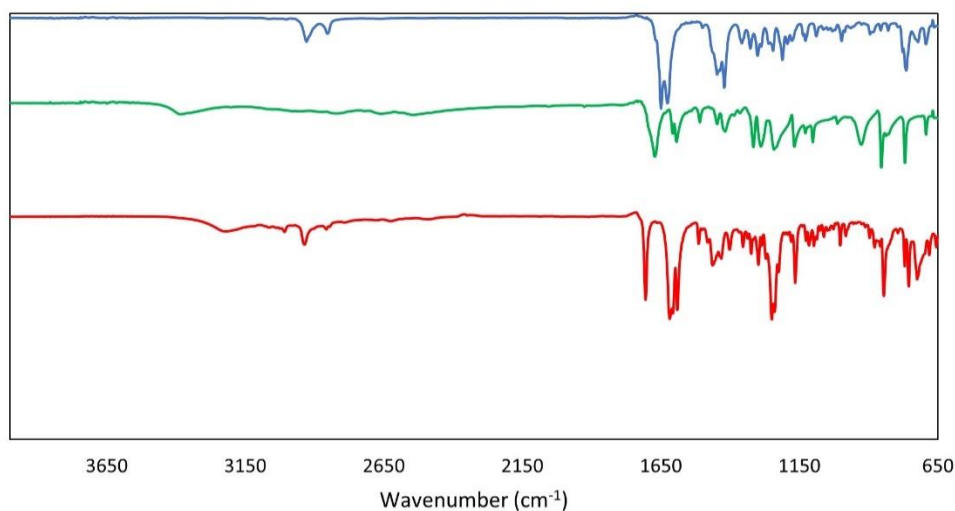


Figure 26 FTIR-ATR spectra for PZQ (in blue), 4-HBZ (in green) and PZQ·4-HBZ (in red).

2.6.4 DSC-TGA and HSM

According to the DSC-TGA trace, presented in Figure 27a, an exothermic peak with marginal mass gain is detected for at approx. 55 °C that is, probably, associated with humidity at sample' surface. In this case, it would be useful to perform an PXRD-VT to elucidate this phenomenon. Melting is recorded at $T_{max} = 152.4$ °C and the decomposition starts at 221.7 °C. The HSM images (Figure 27b) are in good agreement with the temperature proposed for melting by DSC.

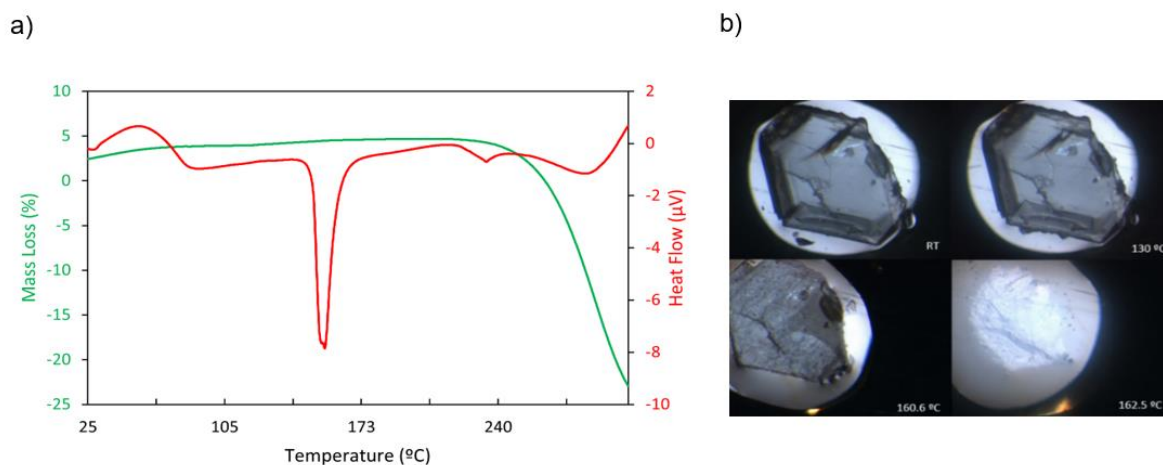


Figure 27 (a) DSC (in red) – TGA (in red) and (b) HSM images for PZQ·4-HBZ.

2.7 PZQ·TRI 1:2

2.7.1 PXRD Analysis

The powder diffractograms for PZQ, TRI and the final product obtained by LAG are presented in Figure 28. The diffractogram of the bulk resulting from the 1:1 grinding experiment showed new peaks as well as some peaks of unreacted starting materials. Starting from this stoichiometry, the SCXRD data suggested that PZQ and TRI reacted in a 1:2 ratio. Hence, the synthetic conditions were optimized for 1:2 stoichiometric composition whose diffraction pattern was in good agreement with the PXRD pattern simulated from the single crystal data. However, despite the formation of 1:2 cocrystals, it is possible to note some excess of TRI, leading to the conclusion that the bulk was not the pure cocrystal, and further optimization of the synthetic conditions would be needed. For this reason, no DSC-TGA experiments were performed.

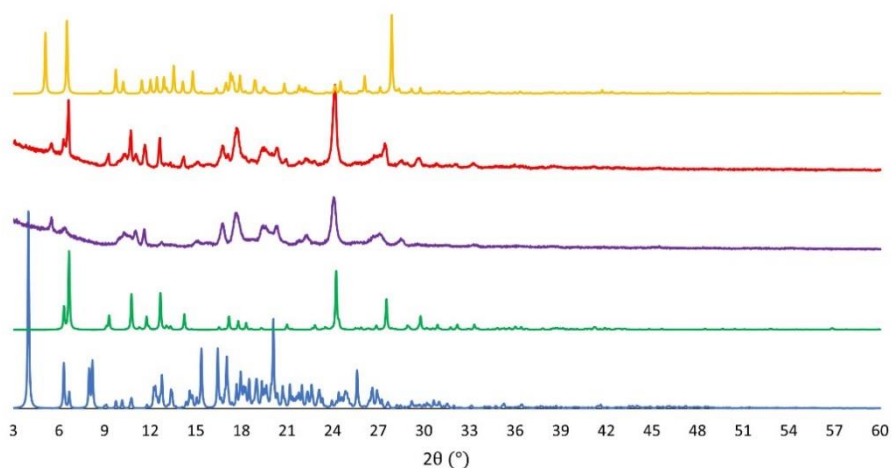


Figure 28 PXRD patterns for the following samples: PZQ (in blue), TRI (in green), PZQ·TRI prepared by LAG with acetonitrile with 1:1 stoichiometry (in purple), PZQ·TRI prepared by LAG with acetonitrile with 1:2 stoichiometry (in red) and the pattern of PZQ·TRI 1:2 simulated from the SCXRD analysis (in yellow).

2.7.2 SCXRD Analysis

This new form provided single crystals that were not reported yet, therefore, the structural elucidation was also performed. The illustration of intermolecular interactions and the crystal packing of PZQ·TRI 1:2 is presented in Figure 29. The asymmetric unit of PZQ·TRI 1:2 consists of one molecule of PZQ, two of TRI and two of water. The intermolecular H-bonds in this cocrystal are presented in Figure 29a, evidencing the $R_2^2(8)$ synthons formed between the carboxylic acids from TRI (i.e., $O_6-H_6\cdots O_8$ 2.545(9) Å and $O_7-H_7\cdots O_5$ 2.573(10) Å). TRI has the capacity to form three $R_2^2(8)$ synthons between each other, however, in this cocrystal dihydrate, only two are formed while the other is disrupted to give rise to the interaction with PZQ and the water molecules. The intermolecular H-bonds also form $D_1^1(2)$ synthons that are established between the $O-H_{H_2O}$ and the $C=O_{COOH}$ from TRI ($O_{10}-H_{10}\cdots O_{2W}$ 2.490(14) Å); one of $O-H_{COOH}$ from the coformer bonds to the carbonyl of the amide group (from PZQ) ($O_3-H_3\cdots O_2$

2.548(10) Å); the remaining bonds are the ones that form the $R_2^2(8)$ synthon. The supramolecular crystal packing is presented in Figure 29b, showing that the molecules are organized in layers, in which these layers are connected by the water molecules. Hydrogen bond details for PZQ·TRI 1:2 are given in Table 13.

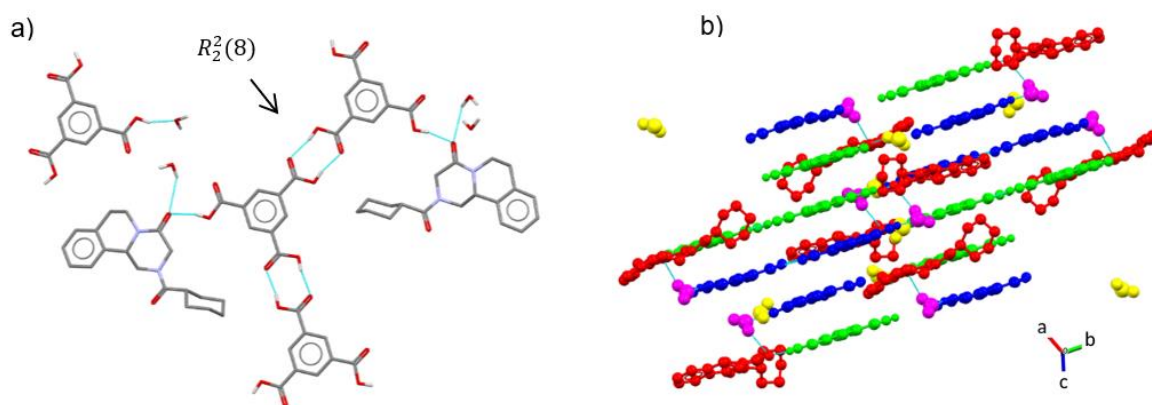


Figure 29 (a) Intermolecular hydrogen bonds in PZQ·TRI 1:2 cocrystal dihydrate; (b) supramolecular crystal packing of PZQ molecules (in red), TRI (in blue and green) and water (in magenta and yellow). All non-contact H atoms were omitted for clarity.

Table 13 List of the main hydrogen bonds found for compound PZQ·TRI 1:2.

Sym. Op.	D–H...A	<i>d</i> (D–H) (Å)	<i>d</i> (H...A) (Å)	<i>d</i> (D...A) (Å)	(DHA) (°)
<i>x</i> , <i>y</i> , <i>z</i>	O _{1W} –H _{1W} ...O ₉	0.87	2.41	2.867(17)	113
<i>x</i> , <i>y</i> , <i>z</i>	O _{1W} –H _{2W} ...O ₂	0.87	2.35	3.075(19)	141
<i>x</i> , <i>y</i> , <i>z</i>	O _{1W} –H _{2W} ...O ₄	0.87	2.47	2.916(17)	112
<i>x</i> , <i>y</i> , <i>z</i>	O ₃ –H ₃ ...O ₂	0.82	1.75	2.548(10)	165
1– <i>x</i> , 1– <i>y</i> , 1– <i>z</i>	O _{2W} –H _{4W} ...O ₂	0.82	2.58	3.34(2)	154
–½+ <i>x</i> , ¾– <i>y</i> , –½+ <i>z</i>	O ₆ –H ₆ ...O ₈	0.82	1.74	2.545(9)	168
½+ <i>x</i> , ¾– <i>y</i> , ½+ <i>z</i>	O ₇ –H ₇ ...O ₅	0.82	1.76	2.573(10)	170
<i>x</i> , <i>y</i> , <i>z</i>	O ₁₀ –H ₁₀ ...O _{2W}	0.82	1.72	2.490(14)	157
½+ <i>x</i> , ½– <i>y</i> , ½+ <i>z</i>	O ₁₁ –H ₁₁ ...O ₁₃	0.82	1.75	2.559(10)	172
–½+ <i>x</i> , ½– <i>y</i> , –½+ <i>z</i>	O ₁₄ –H ₁₄ ...O ₁₂	0.82	1.79	2.606(10)	172

2.7.3 IR Spectroscopy

The FTIR-ATR spectrum of PZQ, TRI and PZQ·TRI 1:2 is presented in Figure 30, showing the formation of the cocrystal. The peaks at 1618 and 1602 cm^{–1} can be attributed to carbonyl stretching vibrations of the amide groups while the peaks at 1720 and 1695 cm^{–1} are related to the carbonyl stretching vibration caused by the carboxylic groups of the coformer. Also, the intermolecular and intramolecular H-bonding are represented by broad band at 3064–3012 cm^{–1} (Table S2). This assignment confirms the cocrystal structure presented in Figure 29.

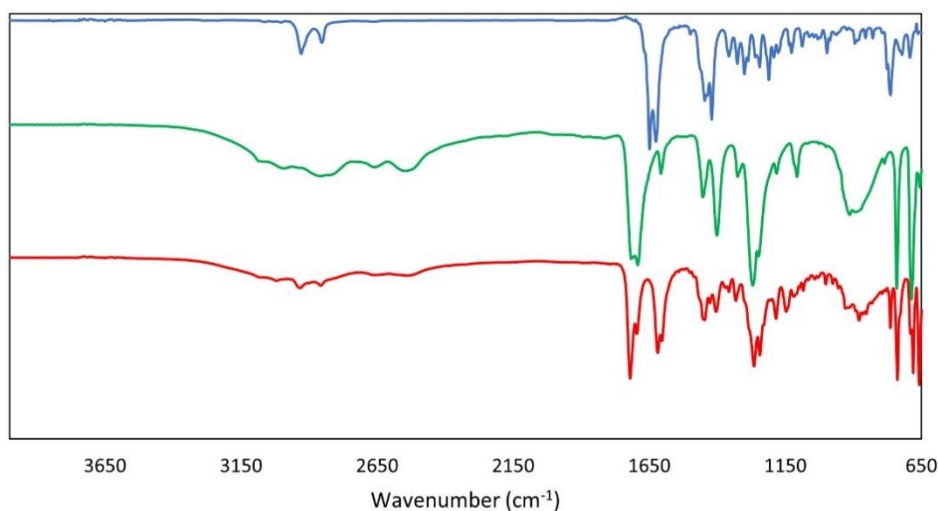


Figure 30 FTIR-ATR spectra for PZQ (in blue), TRI (in green) and PZQ-TRI 1:2 (in red).

2.8 PZQ-5-HIP

2.8.1 PXRD Analysis

The powder diffractograms for PZQ, 5-HIP and the final bulk acquired after LAG are presented in Figure 31. The pattern for the 1:1 combination of PZQ and 5-HIP does not contain peaks of residual starting materials, suggesting the formation of a 1:1 cocrystal for PZQ-5-HIP. Nevertheless, this compound did not provide, so far, single crystals suitable for SCXRD analysis, making it not possible to propose the cocrystal structure and, therefore, the simulation of any powder pattern for comparison with the 1:1 powder resultant from the grinding experiment. For this reason, no DSC-TGA experiments were performed.

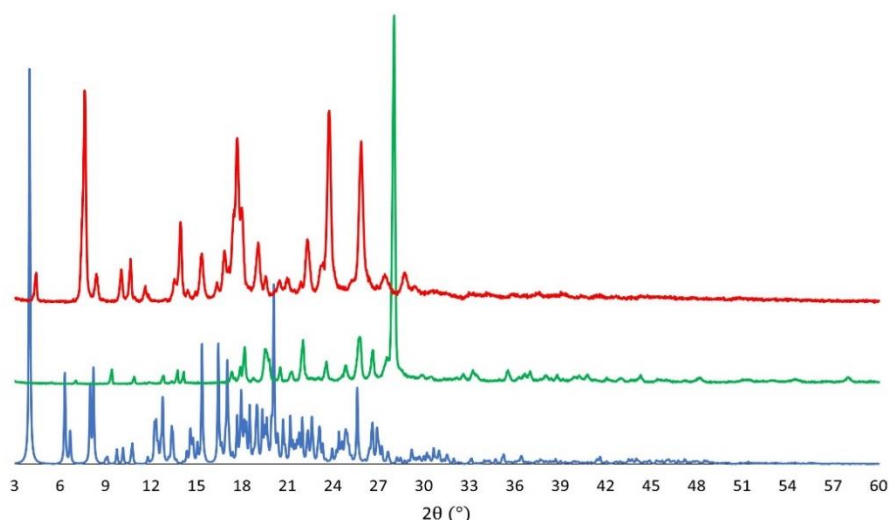


Figure 31 PXRD patterns for the following samples: PZQ (in blue), 5-HIP (in green) and PZQ-5-HIP prepared by LAG with acetonitrile with 1:1 stoichiometry (in red).

2.8.2 IR Spectroscopy

Despite not having the full structure elucidation for the new cocrystal, FTIR-ATR experiments were performed, as the powder proved to be stable on-shelf. The IR spectrum of PZQ-5-HIP and its reagents are presented in Figure 32. The formation of a new cocrystal is not completely evident, because the reagents spectra slightly overlay with PZQ-5-HIP. However, the peaks at 1594 and 1591 cm^{-1} are possibly related to the carbonyl stretching vibrations of the amide groups while the peak at 1670 and 1650 cm^{-1} can be related to the carbonyl stretching vibration caused by the interactions with the carboxylic groups of the coformer.

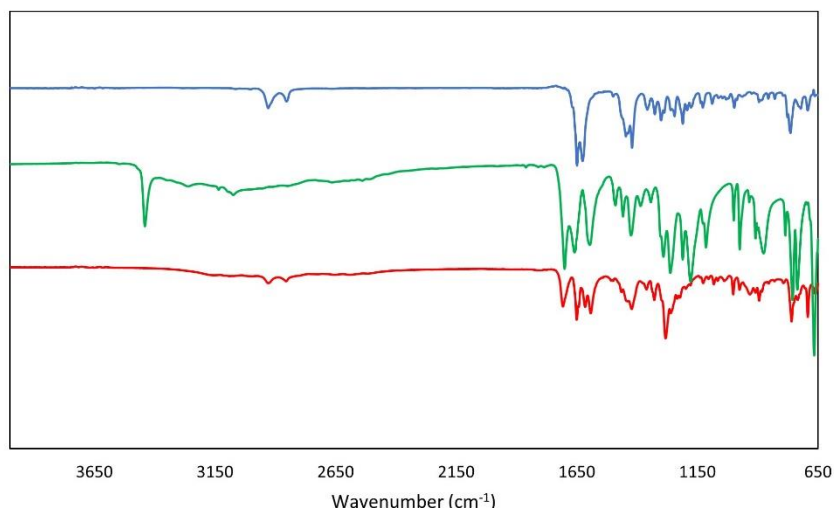


Figure 32 FTIR-ATR spectra for PZQ (in blue), 5-HIP (in green) and PZQ-5-HIP (in red).

2.9 PZQ-MUC

2.9.1 PXRD Analysis

The diffractograms for PZQ, MUC and the final product obtained by LAG are presented in Figure 33. The pattern for the 1:1 combination of PZQ and MUC contains a small peak of residual PZQ, however it can be assumed the formation of a 1:1 cocrystal for these two reagents. As for PZQ-5-HIP, this compound did not provide any single crystals suitable for SCXRD analysis, making it not possible to propose the cocrystal structure. Therefore, it was not possible to simulate of any powder pattern for comparison with the 1:1 powder resultant from the grinding experiment. No FTIR-ATR and DSC-TGA experiments were performed due to the powder not being in the pure form and the lack of stability on-shelf of the cocrystal.

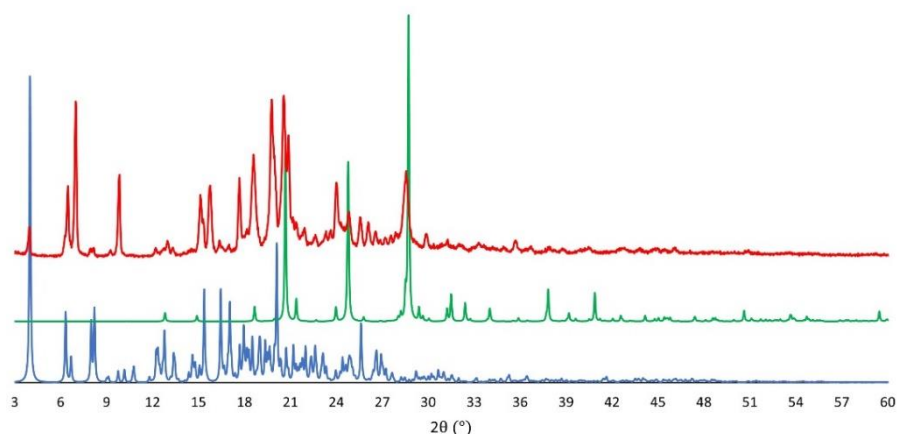


Figure 33 PXRD patterns for the following samples: PZQ (in blue), MUC (in green) and PZQ·MUC prepared by LAG with acetonitrile with 1:1 stoichiometry (in red).

3. Room Humidity Stability Studies

PZQ·4-ASA (Figure 34) and PZQ·MUC (Figure 35) shown to be unstable on-shelf after three and two months after being synthesized, respectively. All the other new crystalline forms were stable on-shelf three months, except for PZQ·TRI 1:2 and PZQ·5-HIP that were stable two months, since they did not show alterations in their PXRD patterns (PXRD diffractograms in Figures S1-7).

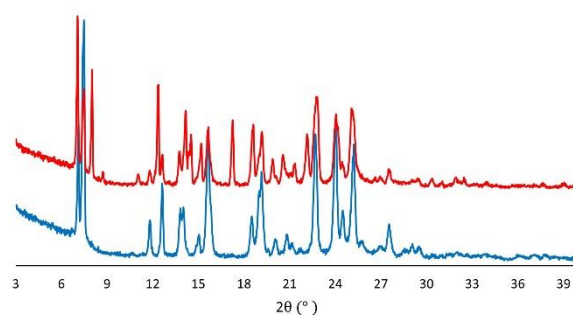


Figure 34 Comparison of PXRD patterns for PZQ·4-ASA (in blue) and PZQ·4-ASA after 3 months (in red) on-shelf.

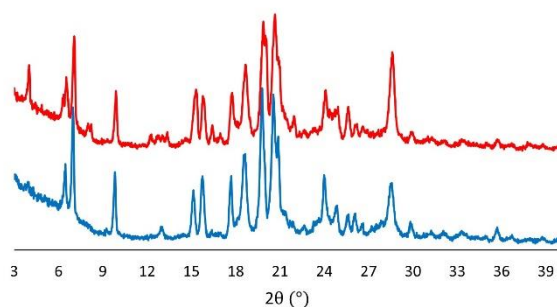


Figure 35 Comparison of PXRD patterns for PZQ·MUC (in blue) and PZQ·MUC after 2 months (in red) on shelf.

In addition, powder stability was also tested at controlled room humidity environments, at storing 90 and 83 % RH content. PZQ·SAL, PZQ·BTC 2:1, PZQ·VAN, PZQ·3-HBZ 2:1 and PZQ·4-HBZ were stable for both humidity environments for 70 days (PXRD diffractograms in Figures S8-21). PZQ·TRI 1:2 and PZQ·5-HIP were analyzed only after 24 and 48 h within the desiccators, being considered stable in both environments. Despite the lack of stability on-shelf, PZQ·4-ASA room humidity stability studies were also performed, showing alterations in the PXRD patterns after only 24 h for both environments at 90 % RH (Figure 36) and 83 % RH (Figure 37). Stability in these environments was not studied for PZQ·MUC.

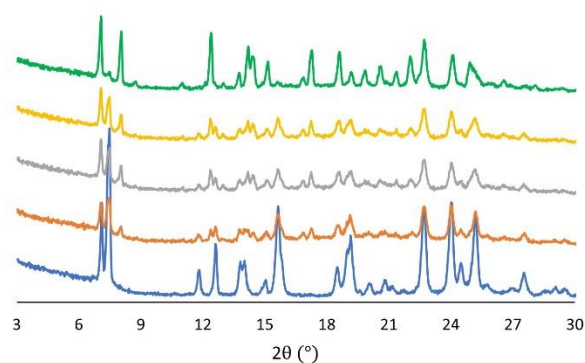


Figure 36 Stability comparison for PZQ·4-ASA (in blue) for 1 (in orange), 2 (in grey), 3 (in yellow) and 7 days (in green) under 90 % RH.

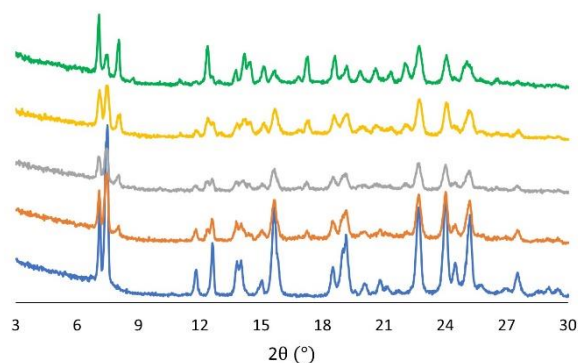


Figure 37 Stability comparison for PZQ·4-ASA (in blue) for 1 (in orange), 2 (in grey), 3 (in yellow) and 7 days (in green) under 83 % RH.

4. Preliminary/ Empirical Solubility Tests

Regarding solubility, this property was evaluated using an empirical method for pure PZQ and for the new compounds that proved stability on-shelf. The preliminary results, presented in Figure 38, show that the aqueous solution of PZQ is the most turbid in comparison with the solutions with cocrystals. PZQ·5-HIP appears to be the most soluble of the studied forms since it required half the amount of water to show the same turbidness. The solubility for 3-HBZ 1:1 was also tested, because it provided a new form different from the single-crystals obtained and, despite not being in a pure form, it showed to also improve the solubility of PZQ. As for the other solutions, it is not possible to rank them from the most to the less soluble because they have the same clarity.

Anyway, these data prove that the new PZQ cocrystal can, indeed, enhance the aqueous solubility of the API. Nevertheless, it is crucial to perform further investigations carrying out HPLC studies to fully characterize the solubility profile of these new PZQ forms.



Figure 38 Solubility comparison for PZQ, PZQ·3-HBZ 2:1, PZQ·4-HBZ, PZQ·TRI 1:2, PZQ·VAN, PZQ·SAL, PZQ·BTC 2:1, PZQ·3-HBZ 1:1 and PZQ·5-HIP (from left to right).

IV. Conclusions

Nine different cocrystals of PZQ were mechanochemically synthesized by LAG. The cocrystals were structurally characterized by PXRD, giving compounds with 1:1 stoichiometry (PZQ·SAL, PZQ·4-ASA, PZQ·4-HBZ, PZQ·VAN, PZQ·5-HIP and PZQ·MUC), 2:1 (PZQ·3-HBZ and PZQ·BTC) and 1:2 stoichiometric ratio (PZQ·TRI). From these nine cocrystals, only two of them, PZQ·5-HIP and PZQ·MUC, did not provide single crystals suitable for SCXRD analysis, being that this technique was used to confirm the structure of the compounds prepared. PZQ·SAL and PZQ·TRI 1:2 formed cocrystal hydrates and dihydrates, respectively, while PZQ·4-ASA provided a cocrystal solvate with acetonitrile.

All coformers that provided cocrystals are benzene rings with at least one carboxylic group, except MUC that is an aliphatic dicarboxylic acid. Some of the coformers tested had also NH₂ groups, because of their capacity for acting as hydrogen bond donors, however, of these coformers, only 4-ASA provided cocrystals with PZQ.

Except for PZQ·MUC, all cocrystals were characterized by FTIR-ATR, which helps to better understand the supramolecular interactions in the crystal structures. This technique confirmed the dominant hydrogen bonding patterns suggested by SCXRD, specially through O-H...O H-bonds between PZQ and carboxylic acids. In PZQ·4-ASA cocrystal solvate, additional N-H...N and N-H...O H-bonds were noted.

Thermal characterization was also performed by DSC-TGA and HSM for the most relevant cocrystals, showing an increase in the melting point for PZQ·4-ASA, PZQ·4-HBZ and PZQ·BTC 2:1 when compared to the literature value⁶⁵ for PZQ alone (136 °C).

One of the aims of this work was to improve PZQ's physicochemical properties, such as solubility and stability. Regarding shelf stability, PZQ·4-ASA and PZQ·MUC were not stable on-shelf after three and two months after being synthesized, respectively, whereas the other cocrystals were stable on-shelf for three months, except for PZQ·TRI 1:2 and PZQ·5-HIP that were stable two months. Regarding RH stability, all forms in which this property was tested, except PZQ·4-ASA, were considered stable in environments with 90 and 83 % RH content. Solubility was evaluated using an empirical method for pure PZQ and for the compounds that proved to be stable on-shelf. This experiment showed that solubility can be increased by the formation of cocrystals, as expected in the beginning of the work, confirming that the physicochemical properties are dependent of the supramolecular structure.

As future work, there are a lot of experiments that can be performed. Beginning with the synthetic procedure, changing the size and number of balls used in the ball mill, as well as the time and frequency of the reaction can lead to an optimization of the process. Same applies to the cocrystals that were not in its pure form. It would also be important to obtain single crystals for the cocrystals which did not provide it for a more complete characterization.

Finally, it would be crucial to perform additional experiments carrying out HPLC studies to fully characterize the solubility profile of these new PZQ forms, as well as to perform antimicrobial activity tests to confirm if these cocrystals can be used as pharmaceutical compounds.

V. References

- (1) Martins, I.; Sardo, M.; Alig, E.; Fink, L.; Schmidt, M.; Mafra, L.; Duarte, M. Enhancing Adamantylamine Solubility Through Salt Formation: Novel Products Studied By X-Ray Diffraction And Solid-State NMR. *Crystal Growth & Design* 2019, 19 (3), 1860-1873.
- (2) Kalepu, S.; Nekkanti, V. Insoluble Drug Delivery Strategies: Review Of Recent Advances And Business Prospects. *Acta Pharmaceutica Sinica B* 2015, 5 (5), 442-453.
- (3) Pindelska, E.; Sokal, A.; Kolodziejewski, W. Pharmaceutical Cocrystals, Salts And Polymorphs: Advanced Characterization Techniques. *Advanced Drug Delivery Reviews* 2017, 117, 111-146.
- (4) Loftsson, T.; Brewster, M. Pharmaceutical Applications Of Cyclodextrins: Basic Science And Product Development. *Journal of Pharmacy and Pharmacology* 2010, 62 (11), 1607-1621.
- (5) Schultheiss, N.; Newman, A. Pharmaceutical Cocrystals And Their Physicochemical Properties. *Crystal Growth & Design* 2009, 9 (6), 2950-2967.
- (6) Sarma, B.; Chen, J.; Hsi, H.; Myerson, A. Solid Forms Of Pharmaceuticals: Polymorphs, Salts And Cocrystals. *Korean Journal of Chemical Engineering* 2011, 28 (2), 315-322.
- (7) Lee, E. A Practical Guide To Pharmaceutical Polymorph Screening & Selection. *Asian Journal of Pharmaceutical Sciences* 2014, 9 (4), 163-175.
- (8) Healy, A.; Worku, Z.; Kumar, D.; Madi, A. Pharmaceutical Solvates, Hydrates And Amorphous Forms: A Special Emphasis On Cocrystals. *Advanced Drug Delivery Reviews* 2017, 117, 25-46.
- (9) Shemchuk, O.; André, V.; Duarte, M.; Braga, D.; Grepioni, F. Mechanochemical Preparation Of Molecular And Ionic Co-Crystals Of The Hormone Melatonin. *CrystEngComm* 2019, 21 (18), 2949-2954.
- (10) Braga, D.; Grepioni, F.; Shemchuk, O. Organic-Inorganic Ionic Co-Crystals: A New Class Of Multipurpose Compounds. *CrystEngComm* 2018, 20 (16), 2212-2220.
- (11) Kumar, S.; Nanda, A. Pharmaceutical Cocrystals: An Overview. *Indian Journal of Pharmaceutical Sciences* 2017, 79 (6).
- (12) Almarsson, Ö.; Zaworotko, M. Crystal Engineering Of The Composition Of Pharmaceutical Phases. Do Pharmaceutical Co-Crystals Represent A New Path To Improved Medicines?. *Chemical Communications* 2004, No. 17, 1889.
- (13) Desiraju, G. Crystal Engineering: From Molecule To Crystal. *Journal of the American Chemical Society* 2013, 135 (27), 9952-9967.
- (14) Duggirala, N.; Perry, M.; Almarsson, Ö.; Zaworotko, M. Pharmaceutical Cocrystals: Along The Path To Improved Medicines. *Chemical Communications* 2016, 52 (4), 640-655.
- (15) Generally Recognized as Safe (GRAS). <https://www.fda.gov/food/food-ingredients-packaging/generally-recognized-safe-gras> (accessed Oct 8, 2021).

- (16) Braga, D.; Maini, L.; Grepioni, F. Mechanochemical Preparation Of Co-Crystals. *Chemical Society Reviews* 2013, 42 (18), 7638.
- (17) Morissette, S. High-Throughput Crystallization: Polymorphs, Salts, Co-Crystals And Solvates Of Pharmaceutical Solids. *Advanced Drug Delivery Reviews* 2004, 56 (3), 275-300.
- (18) Jain, A.; Yang, G.; Yalkowsky, S. Estimation Of Melting Points Of Organic Compounds. *Industrial & Engineering Chemistry Research* 2004, 43 (23), 7618-7621.
- (19) Sathisaran, I.; Dalvi, S. Engineering Cocrystals Of Poorly Water-Soluble Drugs To Enhance Dissolution In Aqueous Medium. *Pharmaceutics* 2018, 10 (3), 108.
- (20) Kuminek, G.; Cao, F.; Bahia de Oliveira da Rocha, A.; Gonçalves Cardoso, S.; Rodríguez-Hornedo, N. Cocrystals To Facilitate Delivery Of Poorly Soluble Compounds Beyond-Rule-Of-5. *Advanced Drug Delivery Reviews* 2016, 101, 143-166.
- (21) Martin, F.; Pop, M.; Borodi, G.; Filip, X.; Kacso, I. Ketoconazole Salt And Co-Crystals With Enhanced Aqueous Solubility. *Crystal Growth & Design* 2013, 13 (10), 4295-4304.
- (22) Rodríguez-Hornedo, N.; Nehm, S.; Seefeldt, K.; Pagán-Torres, Y.; Falkiewicz, C. Reaction Crystallization Of Pharmaceutical Molecular Complexes. *Molecular Pharmaceutics* 2006, 3 (3), 362-367.
- (23) Karimi-Jafari, M.; Padrela, L.; Walker, G.; Croker, D. Creating Cocrystals: A Review Of Pharmaceutical Cocrystal Preparation Routes And Applications. *Crystal Growth & Design* 2018, 18 (10), 6370-6387.
- (24) Douroumis, D.; Ross, S.; Nokhodchi, A. Advanced Methodologies For Cocrystal Synthesis. *Advanced Drug Delivery Reviews* 2017, 117, 178-195.
- (25) Nishio, M. CH/? Hydrogen Bonds In Crystals. *CrystEngComm* 2004, 6 (27), 130.
- (26) Etter, M. Hydrogen Bonds As Design Elements In Organic Chemistry. *The Journal of Physical Chemistry* 1991, 95 (12), 4601-4610.
- (27) Fleischman, S.; Kuduva, S.; McMahon, J.; Moulton, B.; Bailey Walsh, R.; Rodríguez-Hornedo, N.; Zaworotko, M. Crystal Engineering Of The Composition Of Pharmaceutical Phases: Multiple-Component Crystalline Solids Involving Carbamazepine. *Crystal Growth & Design* 2003, 3 (6), 909-919.
- (28) Desiraju, G. Supramolecular Synthons In Crystal Engineering—A New Organic Synthesis. *Angewandte Chemie International Edition in English* 1995, 34 (21), 2311-2327.
- (29) Walsh, R.; Bradner, M.; Fleischman, S.; Morales, L.; Moulton, B.; Rodríguez-Hornedo, N.; Zaworotko, M. Crystal Engineering Of The Composition Of Pharmaceutical Phases. *Chemical Communications* 2002, No. 2, 186-187.
- (30) Ross, S.; Lamprou, D.; Douroumis, D. Engineering And Manufacturing Of Pharmaceutical Co-Crystals: A Review Of Solvent-Free Manufacturing Technologies. *Chemical Communications* 2016, 52 (57), 8772-8786.

- (31) Vishweshwar, P.; McMahon, J.; Bis, J.; Zaworotko, M. Pharmaceutical Co-Crystals. *Journal of Pharmaceutical Sciences* 2006, 95 (3), 499-516.
- (32) Etter, M.; MacDonald, J.; Bernstein, J. Graph-Set Analysis Of Hydrogen-Bond Patterns In Organic Crystals. *Acta Crystallographica Section B Structural Science* 1990, 46 (2), 256-262.
- (33) The Cambridge Structural Database (CSD) - The Cambridge Crystallographic Data Centre (CCDC). <https://www.ccdc.cam.ac.uk/solutions/csd-core/components/csd/> (accessed Oct 25, 2021).
- (34) Shemchuk, O.; Grepioni, F.; Braga, D. Mechanochemical Preparation And Solid-State Characterization Of 1:1 And 2:1 Ionic Cocrystals Of Cyanuric Acid With Alkali Halides. *Crystal Growth & Design* 2020, 20 (11), 7230-7237.
- (35) Tröbs, L.; Emmerling, F. Mechanochemical Synthesis And Characterisation Of Cocrystals And Metal Organic Compounds. *Faraday Discuss.* 2014, 170, 109-119.
- (36) Friščić, T.; Mottillo, C.; Titi, H. Mechanochemistry For Synthesis. *Angewandte Chemie International Edition* 2019, 59 (3), 1018-1029.
- (37) Gomollón-Bel, F. Ten Chemical Innovations That Will Change Our World: IUPAC Identifies Emerging Technologies In Chemistry With Potential To Make Our Planet More Sustainable. *Chemistry International* 2019, 41 (2), 12-17.
- (38) Ying, P.; Yu, J.; Su, W. Liquid-Assisted Grinding Mechanochemistry In The Synthesis Of Pharmaceuticals. *Advanced Synthesis & Catalysis* 2021, 363 (5), 1246-1271.
- (39) Hernández, J.; Bolm, C. Altering Product Selectivity By Mechanochemistry. *The Journal of Organic Chemistry* 2017, 82 (8), 4007-4019.
- (40) James, S.; Adams, C.; Bolm, C.; Braga, D.; Collier, P.; Friščić, T.; Grepioni, F.; Harris, K.; Hyett, G.; Jones, W.; Krebs, A.; Mack, J.; Maini, L.; Orpen, A.; Parkin, I.; Shearouse, W.; Steed, J.; Waddell, D. Mechanochemistry: Opportunities For New And Cleaner Synthesis. *Chem. Soc. Rev.* 2012, 41 (1), 413-447.
- (41) Takacs, L. The Historical Development Of Mechanochemistry. *Chemical Society Reviews* 2013, 42 (18), 7649.
- (42) Xing, T.; Sunarso, J.; Yang, W.; Yin, Y.; Glushenkov, A.; Li, L.; Howlett, P.; Chen, Y. Ball Milling: A Green Mechanochemical Approach For Synthesis Of Nitrogen Doped Carbon Nanoparticles. *Nanoscale* 2013, 5 (17), 7970.
- (43) Espinosa-Lara, J.; Guzman-Villanueva, D.; Arenas-García, J.; Herrera-Ruiz, D.; Rivera-Islas, J.; Román-Bravo, P.; Morales-Rojas, H.; Höpfl, H. Cocrystals Of Active Pharmaceutical Ingredients—Praziquantel In Combination With Oxalic, Malonic, Succinic, Maleic, Fumaric, Glutaric, Adipic, And Pimelic Acids. *Crystal Growth & Design* 2012, 13 (1), 169-185.
- (44) Andrews, P.; Thomas, H.; Pohlke, R.; Seubert, J. Praziquantel. *Medicinal Research Reviews* 1983, 3 (2), 147-200.

- (45) Sun, D.; Mao, R.; Wang, D.; Hu, C.; Zheng, Y.; Sun, Q. The Cytotoxicity Study Of Praziquantel Enantiomers. *Drug Design, Development and Therapy* 2016, Volume 10, 2061-2068.
- (46) Woelfle, M.; Seerden, J.; de Gooijer, J.; Pouwer, K.; Oliaro, P.; Todd, M. Resolution Of Praziquantel. *PLoS Neglected Tropical Diseases* 2011, 5 (9), e1260.
- (47) Šagud, I.; Zanolli, D.; Perissutti, B.; Passerini, N.; Škorić, I. Identification Of Degradation Products Of Praziquantel During The Mechanochemical Activation. *Journal of Pharmaceutical and Biomedical Analysis* 2018, 159, 291-295.
- (48) Devogelaer, J.; Charpentier, M.; Tijink, A.; Dupray, V.; Coquerel, G.; Johnston, K.; Meekes, H.; Tinnemans, P.; Vlieg, E.; ter Horst, J.; de Gelder, R. Cocrystals Of Praziquantel: Discovery By Network-Based Link Prediction. *Crystal Growth & Design* 2021, 21 (6), 3428-3437.
- (49) Yang, D.; Cao, J.; Heng, T.; Xing, C.; Yang, S.; Zhang, L.; Lu, Y.; Du, G. Theoretical Calculation And Structural Analysis Of The Cocrystals Of Three Flavonols With Praziquantel. *Crystal Growth & Design* 2021, 21 (4), 2292-2300.
- (50) Macrae, C.; Bruno, I.; Chisholm, J.; Edgington, P.; McCabe, P.; Pidcock, E.; Rodriguez-Monge, L.; Taylor, R.; van de Streek, J.; Wood, P. Mercury CSD 2.0– New Features For The Visualization And Investigation Of Crystal Structures. *Journal of Applied Crystallography* 2008, 41 (2), 466-470.
- (51) Bruker AXS: SAINT+, release 6.22. Bruker Analytical Systems: Madison,WI. 2005.
- (52) Bruker AXS: SADABS. Bruker Analytical Systems: Madison,WI. 2005.
- (53) Sheldrick GM. A short history of SHELX. *Acta Crystallographica Section A*. 2008, 64, 112-22.
- (54) Farrugia LJ. WinGX - Version 1.80.05. *J Appl Cryst*. 1999, 32, 837-8.
- (55) Spek A.L. Single-crystal structure validation with the program PLATON. *Journal of Applied Crystallography*. 2003, 36, 7-13.
- (56) Roca-Paixão, L.; Correia, N.; Affouard, F. Affinity Prediction Computations And Mechanosynthesis Of Carbamazepine Based Cocrystals. *CrystEngComm* 2019, 21 (45), 6991-7001.
- (57) Sundaralingam, M.; Jensen, L. Refinement Of The Structure Of Salicylic Acid. *Acta Crystallographica* 1965, 18 (6), 1053-1058.
- (58) Montis, R.; Hursthouse, M. Surprisingly Complex Supramolecular Behaviour In The Crystal Structures Of A Family Of Mono-Substituted Salicylic Acids. *CrystEngComm* 2012, 14 (16), 5242.
- (59) Fujii, K.; Ashida, Y.; Uekusa, H.; Guo, F.; Harris, K. Selective Transformation Pathways Between Crystalline Forms Of An Organic Material Established From Powder X-Ray Diffraction Analysis. *Chemical Communications* 2010, 46 (24), 4264.
- (60) Kozlevčar, B.; Odlazek, D.; Golobič, A.; Pevec, A.; Strauch, P.; Šegedin, P. Complexes With Lignin Model Compound Vanillic Acid. Two Different Carboxylate Ligands In The Same Dinuclear Tetracarboxylate Complex $[\text{Cu}_2(\text{C}_8\text{H}_7\text{O}_4)_2(\text{O}_2\text{CCH}_3)_2(\text{CH}_3\text{OH})_2]$. *Polyhedron* 2006, 25 (5), 1161-1166.

- (61) Clevers, S.; Simon, F.; Sanselme, M.; Dupray, V.; Coquerel, G. Monotropic Transition Mechanism Of M-Hydroxybenzoic Acid Investigated By Temperature-Resolved Second Harmonic Generation. *Crystal Growth & Design* 2013, 13 (8), 3697-3704.
- (62) Du, J.; Stanton, S.; Williams, P.; Ong, J.; Groundwater, P.; Overgaard, J.; Platts, J.; Hibbs, D. Using Electron Density To Predict Synthon Formation In A 4-Hydroxybenzoic Acid: 4,4'-Bipyridine Cocrystal. *Crystal Growth & Design* 2018, 18 (3), 1786-1798.
- (63) Duchamp, D.; Marsh, R. The Crystal Structure Of Trimesic Acid (Benzene-1,3,5-Tricarboxylic Acid). *Acta Crystallographica Section B Structural Crystallography and Crystal Chemistry* 1969, 25 (1), 5-19.
- (64) Bernstein, J.; Leiserowitz, L. Molecular Packing Modes. Part X. The Crystal And Molecular Structures Of trans, Trans-Muconic Acid. *Israel Journal of Chemistry* 1972, 10 (2), 601-612.
- (65) Praziquantel: Uses, Interactions, Mechanism of Action | DrugBank Online. <https://www.drugbank.ca/drugs/DB01058> (accessed Oct 14, 2021).

VI. Supporting Information

Table S1 Crystallographic data of PZQ·SAL, PZQ·4-ASA, PZQ·VAN and PZQ·4-HBZ.

Structure	PZQ·SAL	PZQ·4-ASA	PZQ·VAN	PZQ·4-HBZ
Crystal form, color	Plate-like, colorless	Block-shape, colorless	Needle-like, colorless	Block-shape, colorless
Crystal System	Triclinic	Triclinic	Monoclinic	Triclinic
<i>a</i> (Å)	6.89	7.96	17.60	9.89
<i>b</i> (Å)	13.21	13.71	6.11	10.99
<i>c</i> (Å)	4.47	14.24	23.08	12.16
α (°)	70.53	114.50	90.00	108.22
β (°)	13.21	100.75	90.41	101.83
γ (°)	14.47	101.17	90.00	104.65

Table S2 List of relevant IR bands for the new cocrystals.

Cocrystals	Cocrystal $\tilde{\nu}_{\text{C=O}}$ (amide)	Cocrystal $\tilde{\nu}_{\text{C=O}}$ (COOH)	H-bonds
PZQ·SAL	1592/ 1577	1670	3531-3461
PZQ·4-ASA	1635/ 1610	-	3232
PZQ·BTC 2:1	1592/ 1585	1708	3021-2852
PZQ·VAN	1637	1672	3004-2840
PZQ·3-HBZ 2:1	1631/ 1612	1714	-
PZQ·4-HBZ	1618/ 1591	1704	3209
PZQ·TRI 1:2	1618/ 1602	1720/ 1695	3064-3012

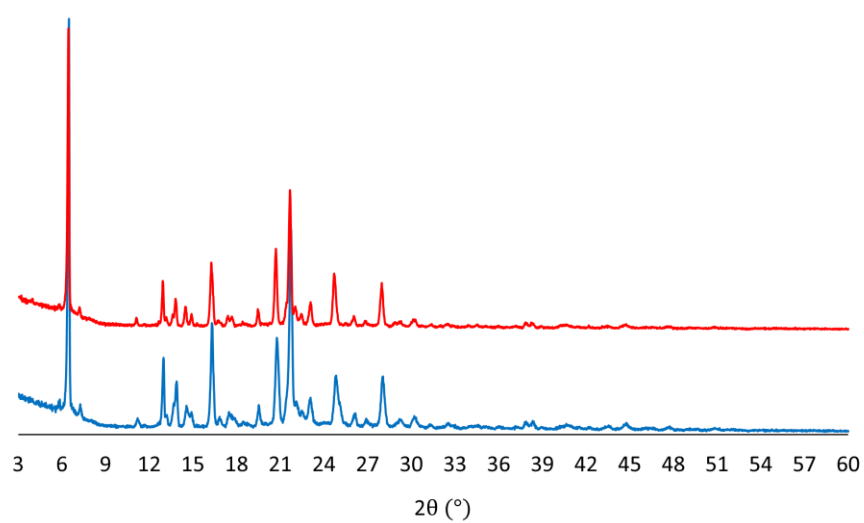


Figure S1 Comparison of PXRD patterns for PZQ·SAL (in blue) and PZQ·SAL after 3 months (in red) on shelf.

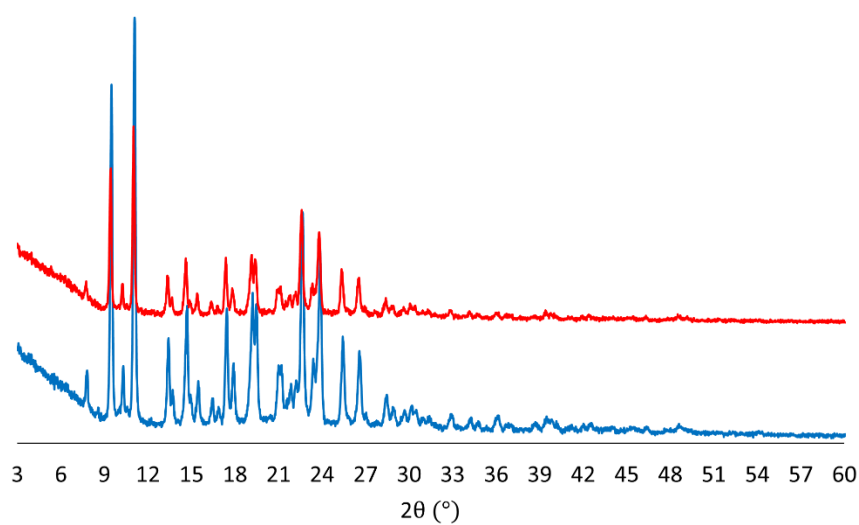


Figure S2 Comparison of PXRD patterns for PZQ·BTC 2:1 (in blue) and PZQ·BTC 2:1 after 3 months (in red) on shelf.

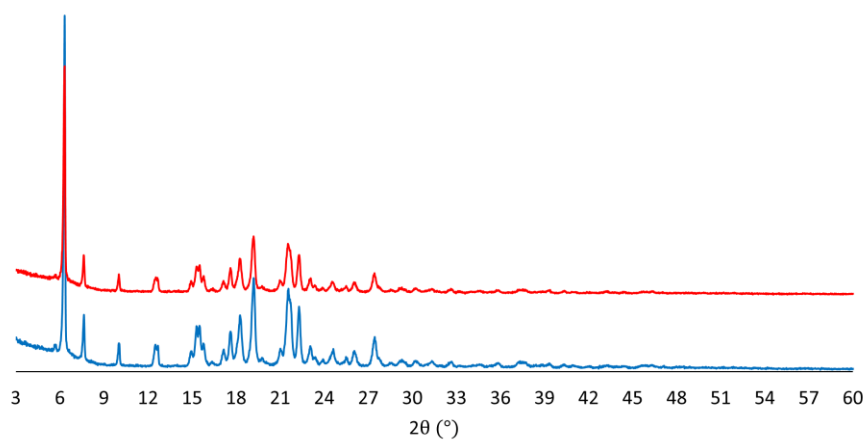


Figure S3 Comparison of PXRD patterns for PZQ·VAN (in blue) and PZQ·VAN after 3 months (in red) on shelf.

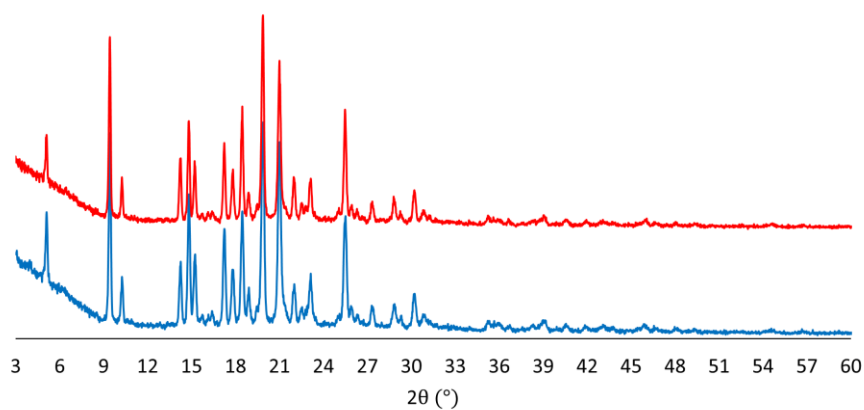


Figure S4 Comparison of PXRD patterns for PZQ·3-HBZ 2:1 (in blue) and PZQ·3-HBZ 2:1 after 3 months (in red) on shelf.

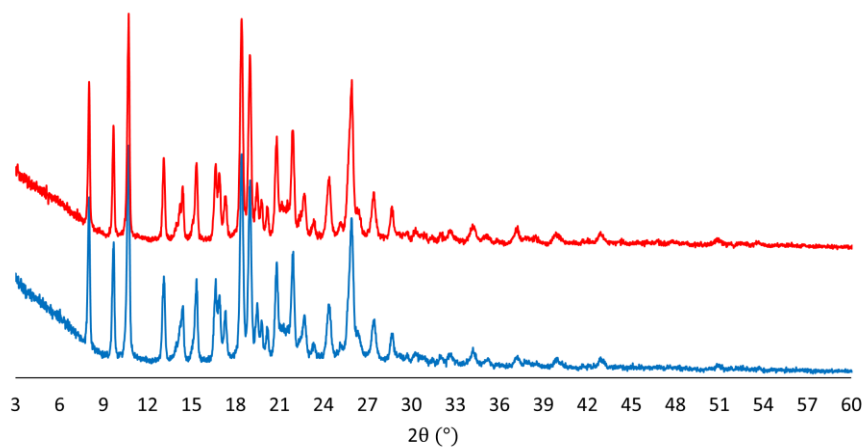


Figure S5 Comparison of PXRD patterns for PZQ·4-HBZ (in blue) and PZQ·4-HBZ after 3 months (in red) on shelf.

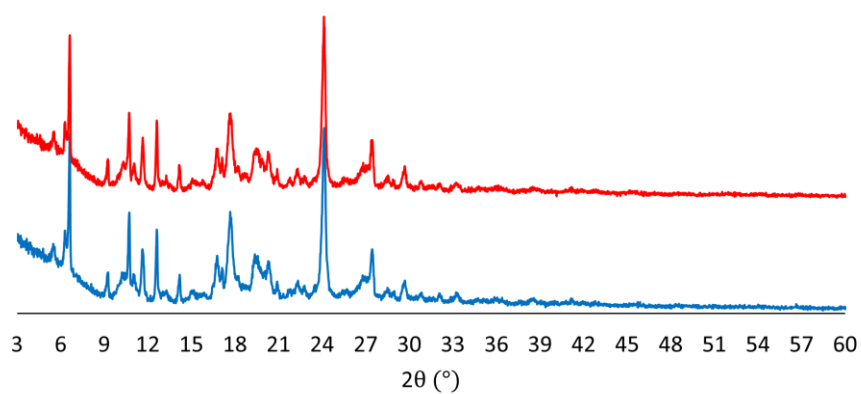


Figure S6 Comparison of PXRD patterns for PZQ·TRI 1:2 (in blue) and PZQ·TRI 1:2 after 2 months (in red) on shelf.

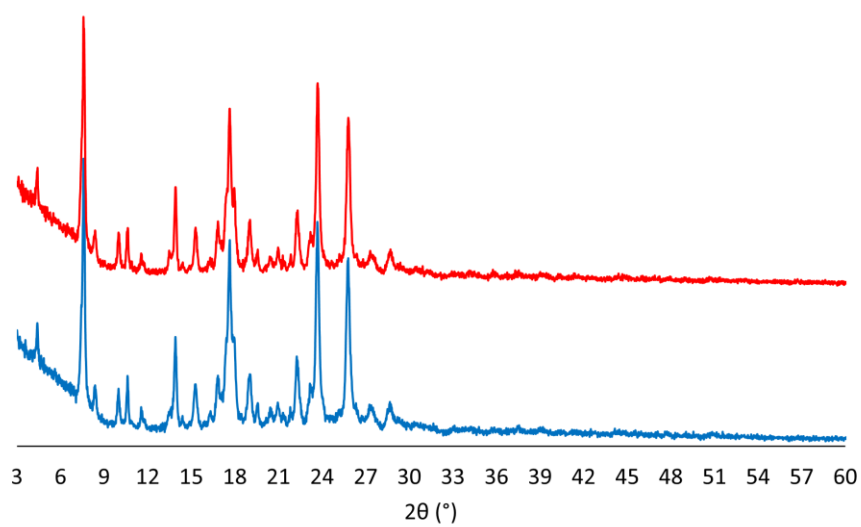


Figure S7 Comparison of PXRD patterns for PZQ·5-HIP (in blue) and PZQ·5-HIP after 2 months (in red) on shelf.

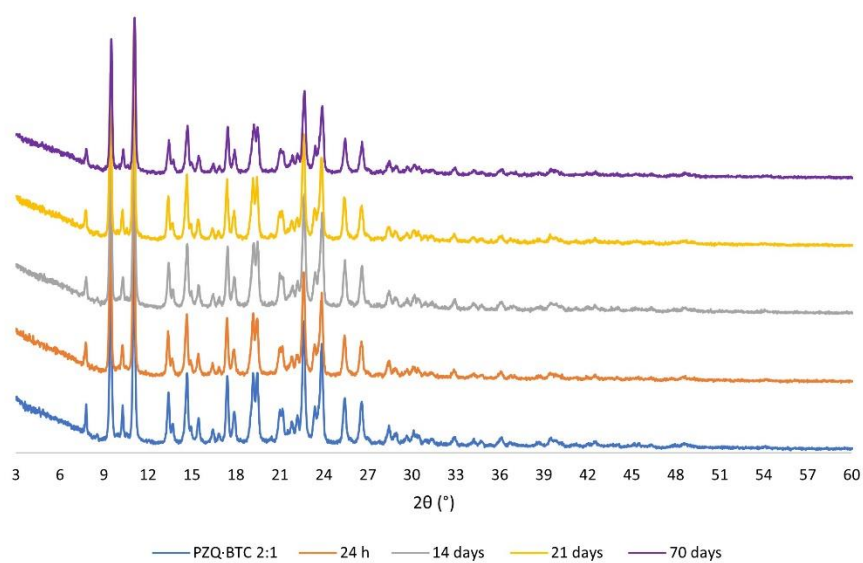


Figure S8 Stability comparison for PZQ·BTC 2:1 for 70 days under 90 % RH.

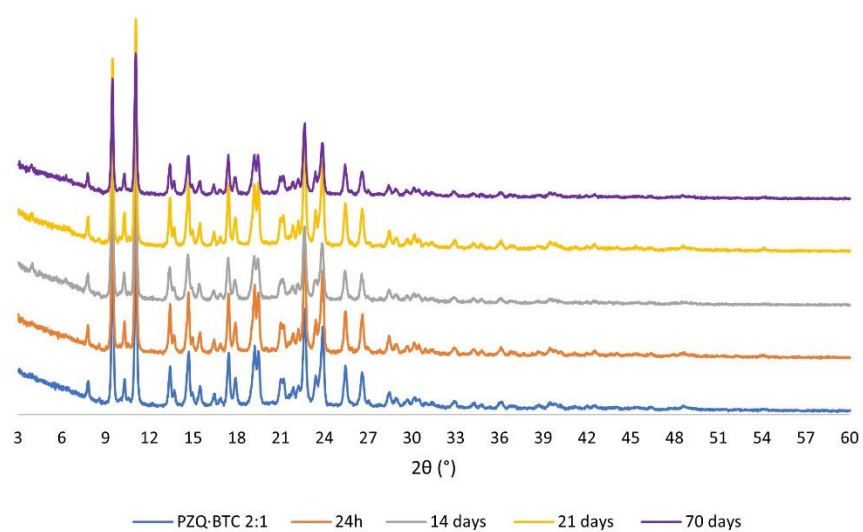


Figure S9 Stability comparison for PZQ·BTC 2:1 for 70 days under 83 % RH.

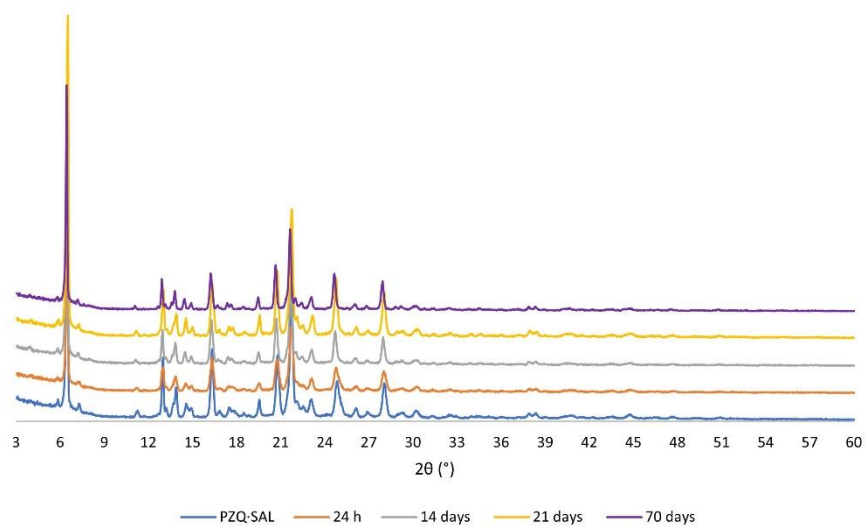


Figure S10 Stability comparison for PZQ·SAL for 70 days under 90 % RH.

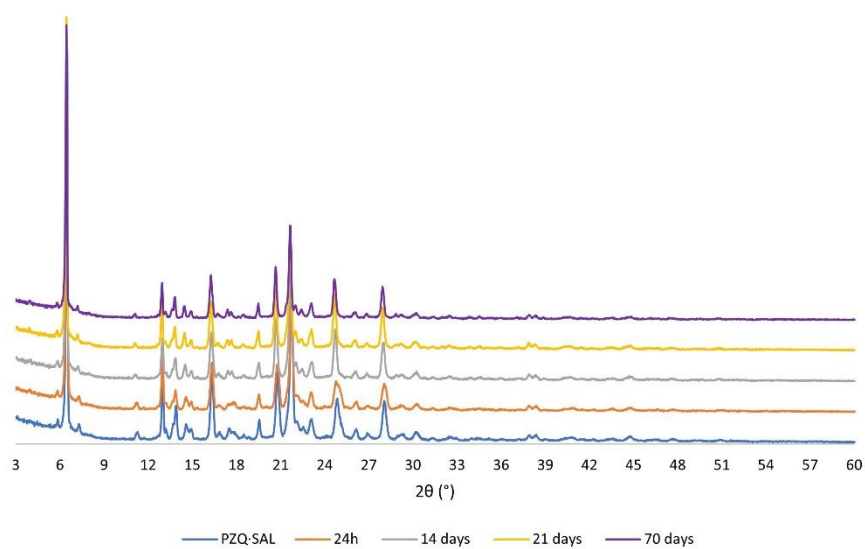


Figure S11 Stability comparison for PZQ·SAL for 70 days under 83 % RH.

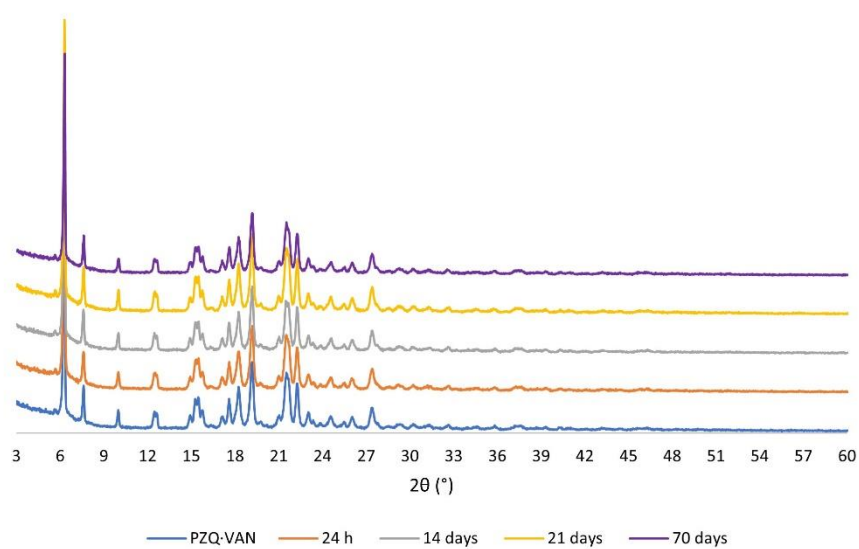


Figure S12 Stability comparison for PZQ·VAN for 70 days under 90 % RH.

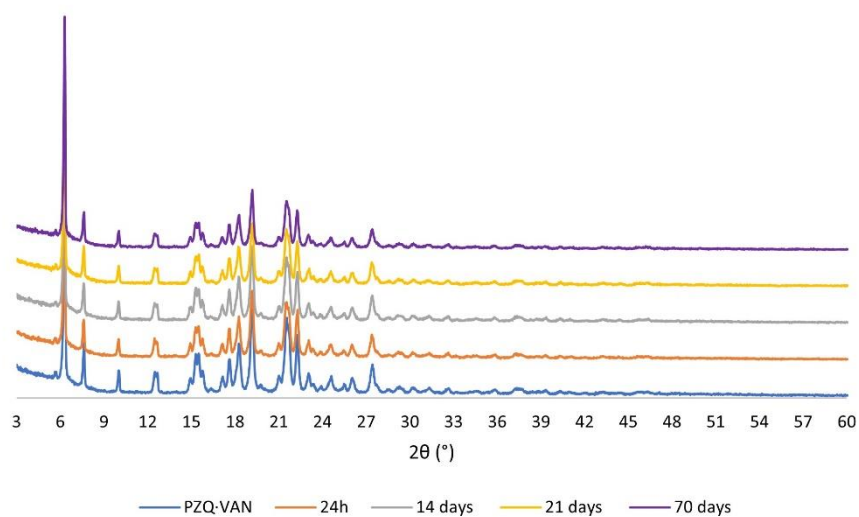


Figure S13 Stability comparison for PZQ·VAN for 70 days under 83 % RH.

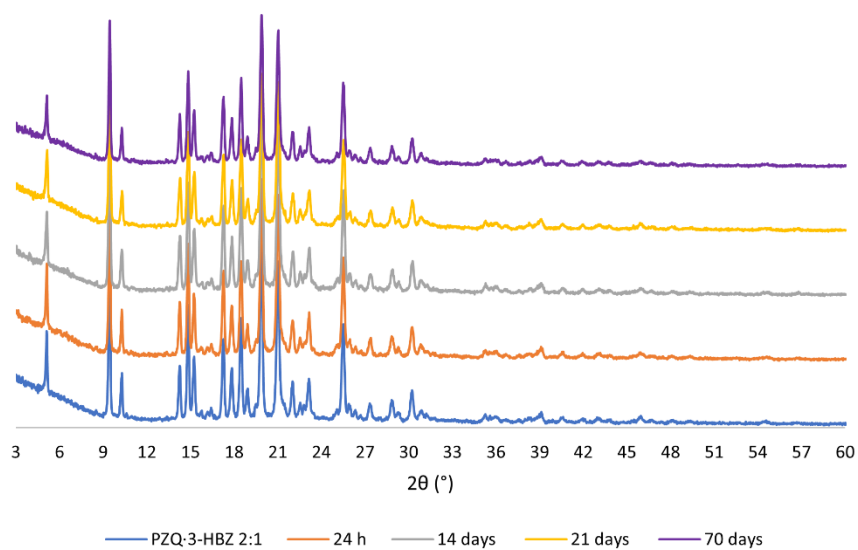


Figure S14 Stability comparison for PZQ·3-HBZ 2:1 for 70 days under 90 % RH.

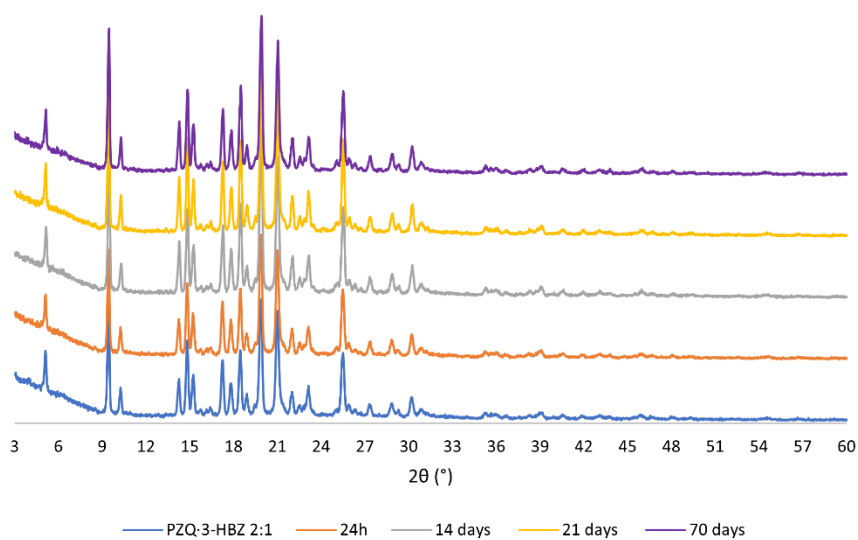


Figure S15 Stability comparison for PZQ·3-HBZ 2:1 for 70 days under 83 % RH.

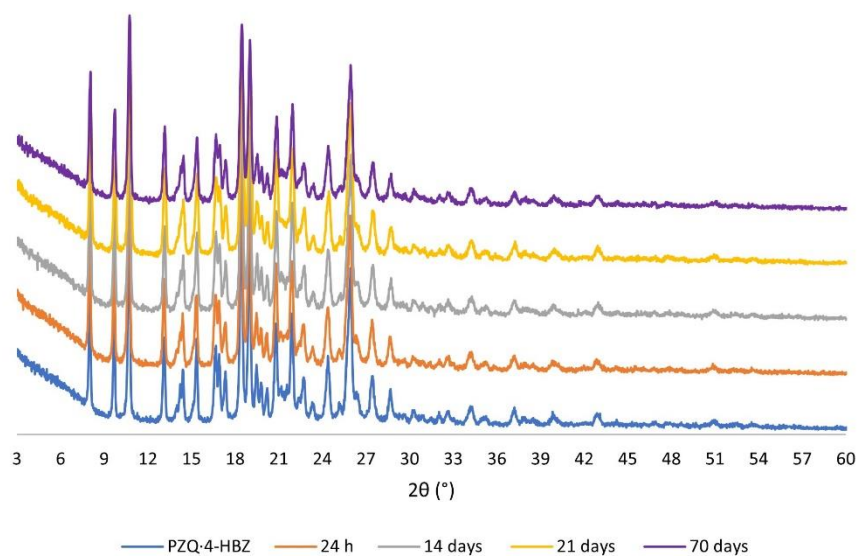


Figure S16 Stability comparison for PZQ-4-HBZ for 70 days under 90 % RH.

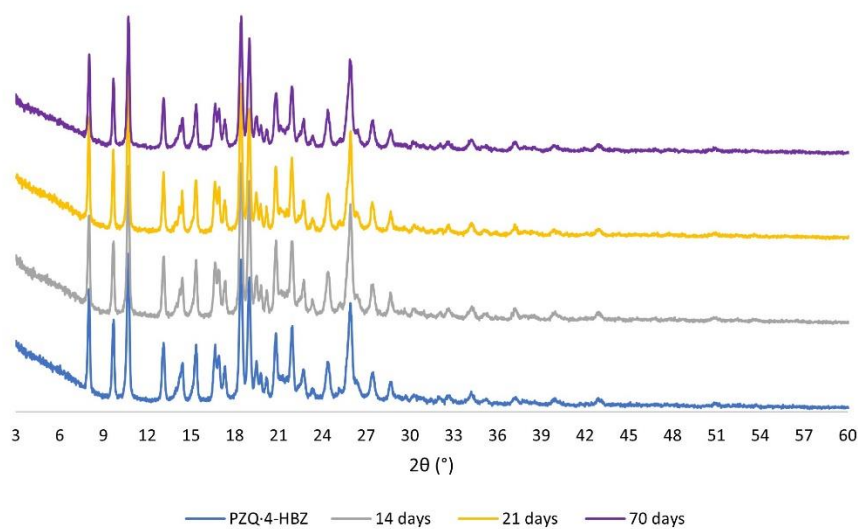


Figure S17 Stability comparison for PZQ-4-HBZ for 70 days under 83 % RH.

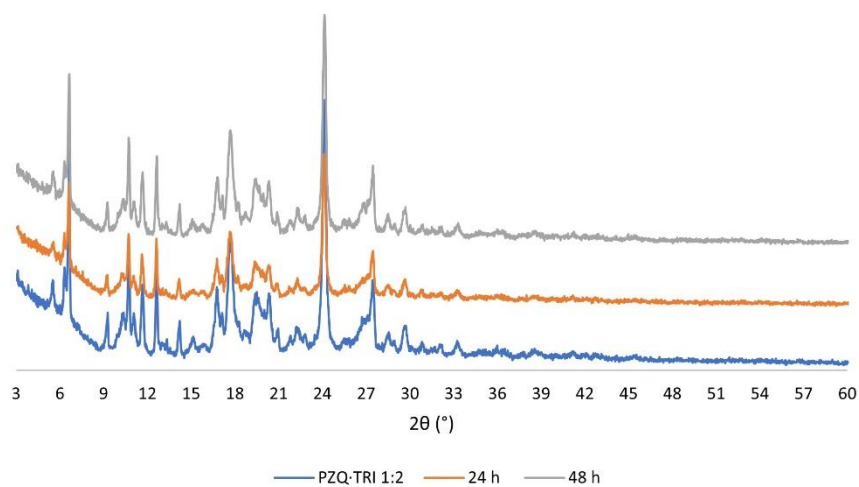


Figure S18 Stability comparison for PZQ-TRI 1:2 for 48 h under 90 % RH.

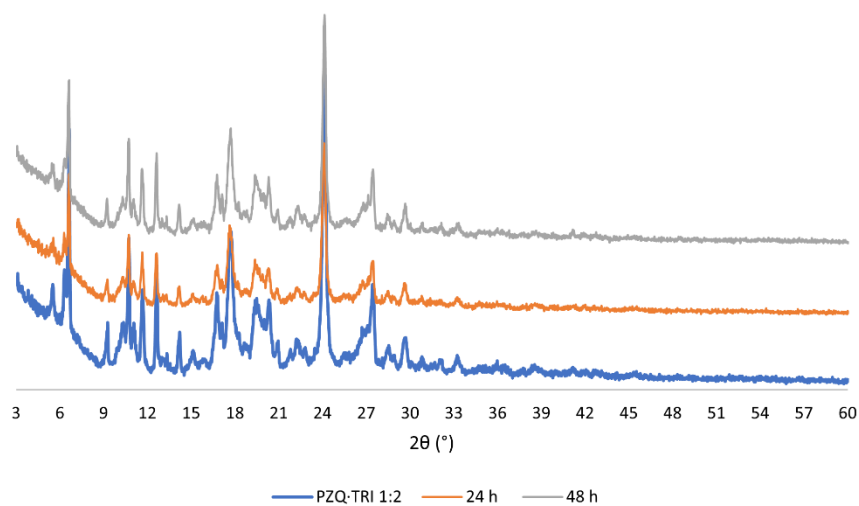


Figure S19 Stability comparison for PZQ-TRI 1:2 for 48 h under 83 % RH.

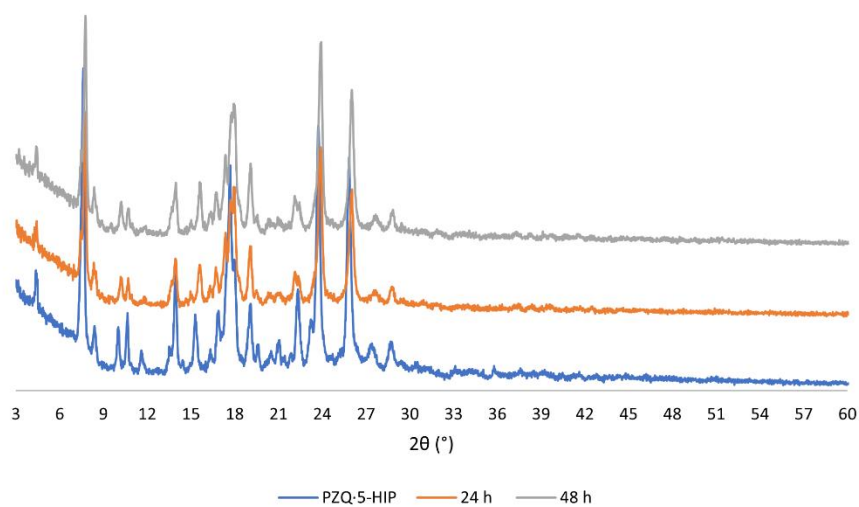


Figure S20 Stability comparison for PZQ-5-HIP for 48 h under 90 % RH.

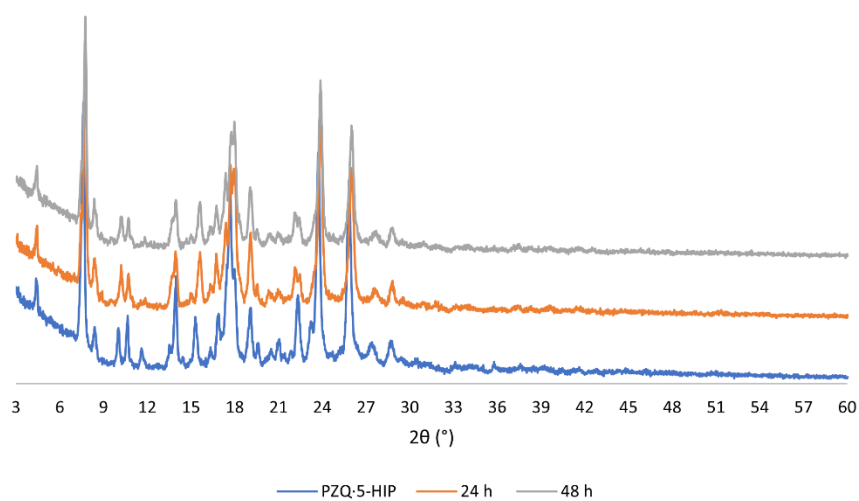


Figure S21 Stability comparison for PZQ-5-HIP for 48 h under 83 % RH.